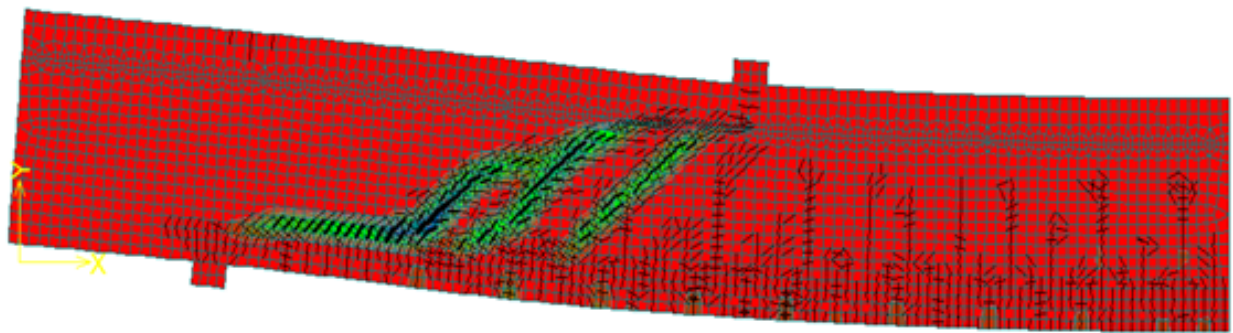


Analytical study on Shear behavior of Composite Concrete Slab



Arjun Vithalkar

Analytical study on Shear behaviour of Composite Concrete Slab

by

Arjun Vithalkar

Additional Thesis report in partial fulfillment of the requirements for the degree of

Master of Science
in Structural Engineering

at the Delft University of Technology,

Student number: 4623894
Supervisor: Dr.ir Yuguang Yang
Committee member: Dr.ir M.A.N.Hendriks

Abstract

Concrete is used significantly in many structures since, the last few centuries. The need to maximize the concrete strength and utilize its complete potential is the main focus of researchers even in today's modern age. It is thus, important to restore the existing structures apart from developing new materials and technology to build new structures. The advancement in scientific research and technology has helped us understand the different mechanisms to strengthen the existing concrete structures such as slabs, beams, bridge decks, walls etc. One such strengthening technique is application of overlays to existing concrete structural elements. An overlay of High Strength Concrete (HSC) above a Normal Strength Concrete (NSC) slab without shear reinforcement, proves to be a successful approach in some cases. One such experimental study is performed by *Dr. Randl* on a composite slab with a HSC overlay on top of NSC Reinforced Concrete (RC) slab. A four point bending test is executed in the experiment on eight such slab specimens. To understand the behaviour of a composite slab undergoing shear failure, an analytical study is performed using three different shear models, Eurocode 2, Critical Shear Crack Theory (CSCT) and Critical Shear Displacement Theory (CSDT). Shear resistances are obtained using these models for each composite concrete slab specimen, considering two separate cases of homogeneous slabs, one with substrate properties and other with overlay concrete properties. The average shear resistances obtained from these two limiting cases are compared with each other and their accuracy with the experimental results is also tested. Furthermore, appropriate guidelines are proposed to evaluate the shear capacity of composite concrete sections with the help of these homogeneous slabs with some validation by a numerical analysis. One shear model among the three, depending on the accuracy of results and the least Coefficient of Variation (COV), is chosen to further give a foundation to the analysis of composite concrete slabs. The composite concrete slab is modeled and a four point bending test is simulated by finite element analysis using ATENA. Although CSDT is developed for homogeneous cross-sections, in this research CSDT provides good estimation of shear behaviour for composite slab cross-section. The theory also explains the experimental results better than any other analytical model with an accuracy of almost 90 % with the least COV of 2.53 %. Crack propagation is observed considering two different homogeneous slab specimens and some changes in the formulae given by CSDT are proposed. A slab factor is also introduced to explain the increase in shear capacity of concrete slab specimen. Effect of bond strength on the shear distribution along the composite slab cross-section is studied with the help of analytical models and equivalent area method. Striking resemblance in the shear stress distribution is observed in case of NSC homogeneous slab and composite concrete slab thus, further validating the idea that shear capacity of a composite concrete slab can be estimated by considering the substrate homogeneous concrete slab properties. Effect of the HSC overlay is not significant in this study. Two limiting cases are considered for further check for de-bonding/delamination of the interface between the two concrete layers. First case with perfect bond and second with no bond between the two concrete layers are considered. No delamination is observed in case of monotonic loading which agrees with the experimental observations as well.

Acknowledgement

My time in TU Delft till now has been very insightful and full of new experiences. The lessons I learnt here, will help me not only until my graduation period but also for the rest of my life. I thank you TU Delft and especially Concrete Structures track for making my dream come true.

First of all, I would like to thank my supervisor **Dr.ir** Yuguang Yang for his support and for providing me with all the resources that were needed during this additional thesis work. His enthusiasm and support in every aspect motivated me to take up this project and successfully carry it to the end. I could understand the finite element software much better because of the knowledge imparted by **Dr.ir** M.A.N.Hendriks. I'm grateful to him for accepting my proposal to be in my additional thesis committee.

I would also like to thank **Dr.ir** Mladena Luković for helping me with some important aspects of my additional thesis work. This really helped me understand the topic more clearly.

Moreover, I would like to thank my friends Prajakta, Srinidhi, Nikhil, Kshiteej, Sakshi, Nilaya, Rucha and Ajinkya for supporting and providing valuable inputs.

Last, but not the least, I would like to thank my sister, brother-in-law and my parents for their trust and continuous support in all the situations. Their love has always motivated me to give my best performance.

List of Figures

2.1	Critical shear crack model: (a) critical section for point loading and distributed loading; (b) determination of longitudinal strain in control depth using internal forces N and M[1]	4
2.2	Shear transfer mechanisms in a free body defined by a flexural crack [2]	5
2.3	Crack profile simplification based on flexural cracks found in shear tests [2]	6
2.4	Calculated critical shear displacement Δ_{cr} against the effective depth d [2]	7
2.5	Flowchart for finding the shear capacity	8
2.6	Crack distribution along section A-A showing average crack variation (dx'_{cr}) and crack length in longitudinal direction (x_{cr})	9
2.7	Simplified model of slab to understand the slab factor ([3])	10
3.1	Reinforcement layout of the test specimens [4]	13
3.2	Preparation of the test plates [4]	14
3.3	Surface treatment and concreting at construction yard [4]	14
3.4	Digital surface models of a rough(left) and smooth(right) specimen section [4]	14
3.5	Test setup for 4-point bending test [4] [all dimensions are in cm]	15
3.6	Actual test setup in the laboratory [4]	15
3.7	Slab cross-sections (a) Composite slab (b) with substrate concrete properties (lower bound) (c) with overlay concrete properties (upper bound)	16
3.8	Modified delta in MATLAB code	21
3.9	Uncoupled members (a) Loading (b) Stress and strain distribution along cross-section	25
3.10	Shear stress distribution in uncoupled members	25
3.11	Coupled members (a) Loading (b) Stress and strain distribution along cross-section	26
3.12	Equivalent area method	26
3.13	Normal and shear stress of concrete in a segment between two primary flexural cracks [5]	27
3.14	Shear stress distribution in coupled members after cracking (for slab no. 8)	28
4.1	Test setup for 4-point bending test [4] [all dimensions are in cm]	31
4.2	Details of test specimen using symmetry (All measurements are in meters)	32
4.3	Finite element model used for analyzing cracking pattern in RC slab with HSC overlay on top	32
5.1	Comparison of shear models (a) Eurocode 2; (b) CSCT; (c) CSDT (Slab factor estimation) (d) CSDT (Slab factor actual calculation)	36
5.2	Comparison of numerical results between Composite slab (Slab no.8) and homogeneous slab	36
5.3	Comparison between experimental (platte 8_Rt=0.8mm) [4] and numerical model (Slab no.8)	37
5.4	Comparison of cracking pattern between experimental and numerical model	38
5.5	Normal and shear stress distribution in numerical model before and after cracking of the shear span	38
5.5	Normal and shear stress distribution in numerical model before and after cracking of the shear span (contd.)	39
5.6	Shear stress distribution in (a) NSC homogeneous slab and (b) HSC homogeneous slab	39
5.7	Shear stress distribution at the interface of the composite concrete slab	40
5.8	Comparison of numerical models with perfect bond and interface properties from experiment	40
B.1	Calculation of various parameters according to CSDT using MATLAB code in A	54
B.2	Relation between $f_{c,cube}$ and $f_{c,cylinder}$ according to Eurocode	55
B.3	Shear force calculations using Eurocode2	56
B.4	Shear force calculations using Critical Shear Crack Theory	57
B.5	Shear force calculations using Critical Shear Displacement Theory	58
B.6	Actual slab factor calculation using CSDT	59

B.7	Comparison of shear force obtained using CSDT (excluding slab factor, including actual slab factor and including estimated slab factor)-1	60
B.8	Comparison of shear force obtained using CSDT (excluding slab factor, including actual slab factor and including estimated slab factor)-2	61
B.9	Calculation of coefficients of variation for all three shear models	62
B.10	RC slab and HSC overlay dimensions as separate and combined elements	63
B.11	Normal stress calculation along the cross-section of uncoupled members	64
B.12	Normal stress calculation along the cross-section of coupled members	65
B.13	Shear stress calculation along the cross-section of uncoupled members	66
B.14	Shear stress calculation along the cross-section of coupled members after crack-1 (using Tung and Tue's theory)	67
B.15	Shear stress calculation along the cross-section of coupled members after crack-2 (using Tung and Tue's theory)	68
B.16	Shear stress along the cross-section of coupled members after crack after some interpolation-1	69
B.17	Shear stress along the cross-section of coupled members after crack after some interpolation-2	70

List of Tables

3.1	Specimen details and respective Load Maxima [4]	15
3.2	Material properties used in experiment	17
3.3	Variation of eurocode model with experimental results (Slab 8)	18
3.4	Variation of eurocode model with experimental results (All slab specimens)	18
3.5	Variation of CSCT model with experimental results (Slab 8)	19
3.6	Variation of CSCT model with experimental results (All slab specimens)	19
3.7	Input parameters and output for lower and upper bound limits using CSDT method (Slab 8)	20
3.8	Variation of CSDT model with experimental results (Slab 8)	20
3.9	Comparison of outputs for lower and upper bound limits using CSDT method excluding and including the slab factor respectively (Slab 8)	22
3.10	Comparison of CSDT model with experimental results (Slab 8) after incorporating the slab factor (SF) (actual calculation)	22
3.11	Comparison of CSDT model with experimental results (Slab 8) after incorporating the slab factor (SF) (approximation)	23
4.1	Material properties of concrete	33
4.2	Material properties of reinforcement	33
4.3	Material properties of interfaces	34
4.4	Material properties of steel plates	34
4.5	Solution parameters	34
4.6	Finite element mesh	34
5.1	Comparison of three shear models with experimental results	35

Contents

List of Figures	7
List of Tables	9
1 Introduction	1
2 Shear Models	3
2.1 Eurocode (EC2)	3
2.2 Critical Shear Crack Theory (CSCT)	3
2.3 Critical Shear Displacement Theory (CSDT)	4
2.3.1 Introduction	4
2.3.2 Simplified Crack Pattern	5
2.3.3 Simplified Shear Force-Displacement Relationship	6
2.3.4 Determination of the Critical Shear Displacement Δ_{cr}	7
2.3.5 Evaluation of Shear Capacity based on Critical Shear Displacement	8
2.3.6 Slab Factor: Influence of specimen width	9
3 Case Study	13
3.1 Preparation of the test specimens	13
3.2 Implementation of four-point bending test	15
3.3 Comparison of shear models based on the input parameters from the case study	16
3.3.1 Procedure for comparison of the shear models	16
3.3.2 Shear resistance calculation using Eurocode	17
3.3.3 Shear resistance calculation using Critical Shear Crack Theory	18
3.3.4 Shear resistance calculation using Critical Shear Displacement Theory	19
3.4 Stress distribution along a critical cross-section of composite concrete slab	24
3.4.1 Concrete-concrete interface shear check	24
4 Numerical Model using ATENA	31
4.1 Numerical Model	32
4.1.1 Introduction on FE Model creation	32
4.1.2 Comments on FE model preparation	32
5 Results and Discussion	35
5.1 Results	35
5.2 Discussion	41
6 Conclusions and Recommendations	43
6.1 Conclusions	43
6.2 Recommendations	44
A CODE for Critical Shear Displacement Theory Method	45
B Excel calculation sheets	53
Bibliography	71

Introduction

Concrete structures have a service life of minimum 40-50 years. Structures built in the early 20th century were designed as per the old design specifications which now, with the advancement in research and technology, have become obsolete. Many of these existing structures are reaching their respective design age. With the increasing demand of road and rail networks, the present structures have to be maintained and repaired as well. With this respect, for example in case of concrete bridges, it is sometimes practically impossible to reconstruct a bridge by demolishing the existing structure. Measures have to be taken to improve the service life of concrete bridges until a better alternative is implemented.

The knowledge regarding the shear capacity of composite concrete slabs is limited until recent times. Here an attempt is made to understand the behaviour of composite concrete slabs undergoing shear failure. Many researchers focus their attention in understanding the shear capacity or shear resistance of a homogeneous concrete slab. Hence, not much literature can be found for heterogeneous cross-section or as described before a composite concrete slab. The discussions in this report mainly include an analytical study performed using different shear theories to understand the shear behaviour and estimate the shear capacity of a composite concrete slab specimen. Furthermore a numerical analysis is performed to validate some of the findings from the analytical study. The model considered is a normal strength (NSC) reinforced concrete (RC) slab with a high strength concrete (HSC) overlay and a four-point loading is applied to understand the failure mode of the slab (in this case a shear failure).

First, a literature review is carried out to understand different shear models used to calculate the shear capacity of a beam or slab element. The three models namely; the Eurocode 2 (EC2) shear model, critical shear crack theory (CSCT) proposed by Muttoni [1] and the critical shear displacement theory (CSDT) proposed by Yang in his report [2], are studied. Eventually, these shear models are applied on a case study specified by Dr. Randl [4]. Based on the experimental results and the input parameters mentioned in the case study, shear resistances with all the three models are calculated. The values obtained from the models are compared with the actual experimental results. The model with the most accurate results is then used for further development of a pertinent numerical model.

The cracking pattern in the homogeneous slabs is compared with the cracking pattern obtained from the numerical analysis of the composite slab specimen. Furthermore, a shear check is performed to observe the behaviour of the interface between the RC concrete slab and the HSC overlay. Two cases are considered; uncoupled and coupled members. These two cases define the limiting values of shear stress capacities for the different range of roughness and cohesion parameters. Normal concrete stress in the tension zone is used to calculate the shear stress at a cracked cross-section for further accuracy. Analytical model proposed by Tung and Tue [5] is also verified with the experimental and numerical model results.

ATENA is a finite element software used specifically to study concrete structures by developing numerical models. The software is used especially in case of concrete structures as it provides ease in developing a structural model with concrete material and gives accurate results while studying the stress-strain properties, creep, shrinkage and strength properties. To further validate the findings of this report, simulations are

run using material properties described in the case study report. In this report, behaviour of a composite concrete slab undergoing four-point bending test is studied. The finite element analysis will thus provide a better view and realistic approximation of a composite concrete structure behaviour.

2

Shear Models

As explained in the previous chapter, the three shear models provide different approaches and distinct parameter relationships to check the shear strength of a concrete member.

- Eurocode
- Critical Shear Crack Theory
- Critical Shear Displacement Method

2.1. EUROCODE (EC2)

As described in NEN-EN 1992-1-1 the shear resistance $V_{Rd,c}$ of a concrete member without shear reinforcement is given by Equation 2.1.

$$V_{Rd,c} = [C_{Rd,c} k (100 \rho_l f_{ck})^{1/3} + k_1 \sigma_{cp}] b_w d \quad (2.1)$$

The minimum value of $V_{Rd,c}$ is given by Equation 2.2.

$$V_{Rd,c} = (v_{min} + k_1 \sigma_{cp}) b_w d \quad (2.2)$$

$$v_{min} = 0.035 k^{3/2} f_{ck}^{1/2} \quad (2.3)$$

In case of shear at the interface concrete cast at different times, shear stress in the interface should satisfy, $v_{Ed,i} \leq v_{Rd,i}$ (Equation 2.5) where, $v_{Ed,i}$ (Equation 2.4) is the design value of the shear stress at the interface

$$v_{Ed,i} = \beta V_{Ed} / (z b_i) \quad (2.4)$$

$$v_{Rd,i} = c f_{ctd} + \mu \sigma_n + \rho f_{yd} (\mu \sin \alpha + \cos \alpha) \leq 0.5 v f_{cd} \quad (2.5)$$

where, c and μ are factors depending on the roughness of the interface.

2.2. CRITICAL SHEAR CRACK THEORY (CSCT)

The Critical Shear Crack Theory developed by Muttoni and Ruiz [1] gives an insight on the shear resistance of concrete members without transverse reinforcement as a function of critical shear crack width. This theory accepts the following hypotheses,

- The shear strength is checked in a section where the width of the critical shear crack can be sufficiently represented by the strain at a depth of $0.6d$ from the compressive face (Figure 9 [1])
- The critical crack width w is proportional to the product of the longitudinal strain in the control depth ε and the effective depth of the member d

$$w \propto \varepsilon d$$

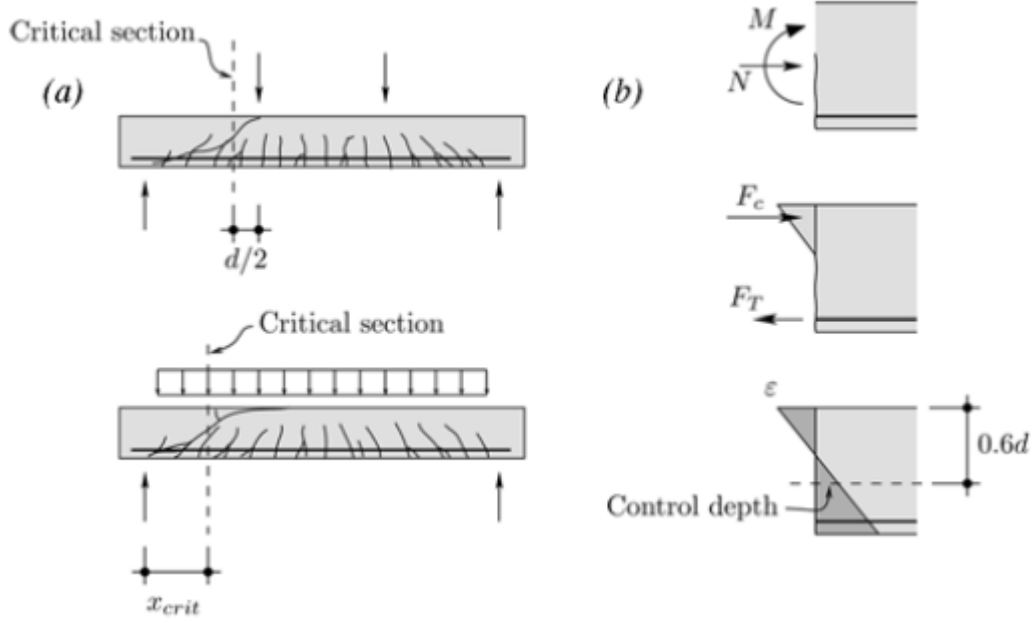


Figure 2.1: Critical shear crack model: (a) critical section for point loading and distributed loading; (b) determination of longitudinal strain in control depth using internal forces N and M [1]

In case when only bending moment M is acting on the critical cross-section without any axial force, strain in the control depth can be derived with the Equation 2.6.

$$\varepsilon = \frac{M}{bd\rho E_s(d-c/3)} \frac{0.6d-c}{d-c} \quad (2.6)$$

where, c the depth of the compression zone is given by Equation 2.7.

$$c = d\rho \frac{E_s}{E_c} \left(\sqrt{1 + \frac{2E_c}{\rho E_s}} - 1 \right) \quad (2.7)$$

where, E_c is taken as $E_c \approx 10000f_c^{1/3}$ in MPa

Finally, shear strength of the member is calculated using the critical crack width, the aggregate size and the concrete compressive strength as given by Equation 2.8.

$$\frac{V_R}{bd\sqrt{f_c}} = \frac{1}{6} \times \frac{2}{1 + 120 \frac{\varepsilon d}{16 + d_g}} \quad (2.8)$$

2.3. CRITICAL SHEAR DISPLACEMENT THEORY (CSDT)

2.3.1. INTRODUCTION

In his research, Yang [2] uses the parameter of critical shear crack displacement for calculating the shear capacity of a reinforced concrete member without shear reinforcement. The model proposes that the opening of the critical inclined crack can be considered as a lower bound for the shear capacity of a structural member. Moreover, the unstable opening of the critical inclined crack is triggered when the shear displacement in an existing flexural crack reaches a critical value Δ_{cr} [2]. There are two types of crack patterns in a concrete member.

- First one is defined as a flexural crack which has two secondary branches, one approaching the support at the level of the tensile reinforcement and the other to the point having maximum rotation in the compression zone. This crack is usually diagonal in nature and is called as a flexural shear crack.
- The second type of crack is a shear compression crack which results from a failure caused by crushing of the concrete in the compression zone.

The Critical Shear Displacement Method (CSDM) considers the flexural shear failure and the relation between the forces in the vicinity of the crack to determine the shear strength of a concrete specimen. The relations established are mainly for concrete beam specimens with large slenderness ratio (a/d more than 3.0) and for beams without transverse reinforcement.

2.3.2. SIMPLIFIED CRACK PATTERN

In this section, a free body is examined by considering different shear transfer mechanisms. It has been generally accepted that if a flexural crack is observed in a concrete beam, the shear force can be transferred by four mechanisms as summarized by ASCE-ACI Committee 445, as shown in Figure 2.2.

- Shear stress transfer in the uncracked compression zone
- Shear stress transferred due to the aggregate interlock across a crack
- Shear transfer due to the dowel action of the longitudinal reinforcement
- Residual tensile stress at the limited crack opening

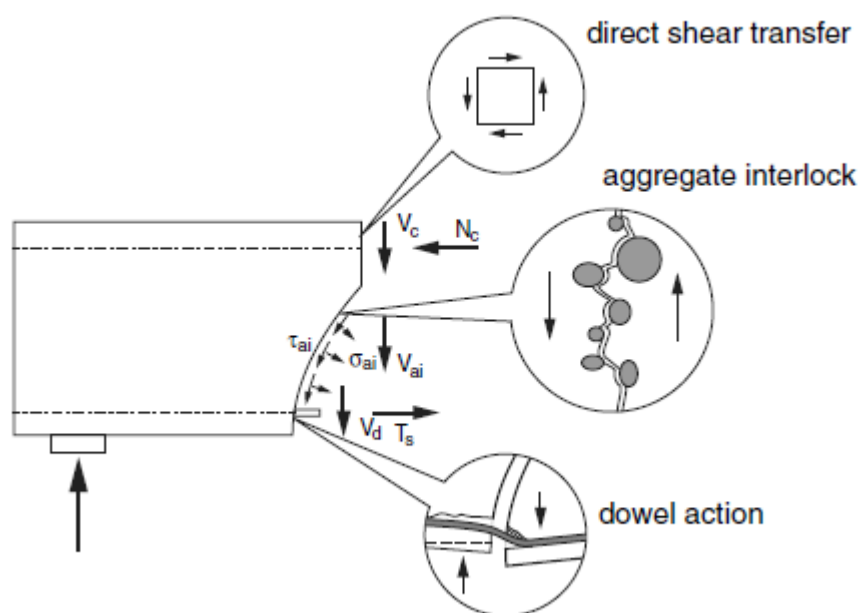


Figure 2.2: Shear transfer mechanisms in a free body defined by a flexural crack [2]

Flexural cracks are distributed almost evenly near the tensile reinforcement. However, due to the stress reduction in the vicinity of the crack, stress reduction takes place and all cracks do not reach the compression zone of the concrete member.

The crack pattern observed in the tests reported in Yang [3] are shown in Figure. 2.2

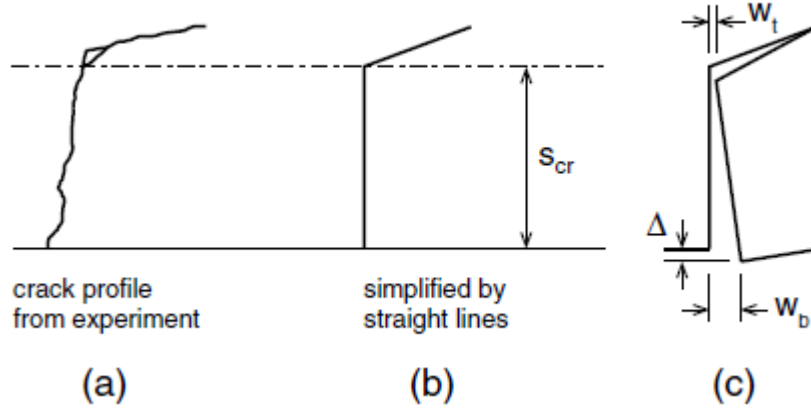


Figure 2.3: Crack profile simplification based on flexural cracks found in shear tests [2]

As Yang's research mainly focuses on cracks at cross sections having large M/Vd values, some simplifications are considered to the crack pattern. The main features of these findings are,

- The crack comprises of two branches: the major part is formed directly after the crack initiates and the secondary branch is in the compression zone.
- The major crack is simplified as being perpendicular to the longitudinal direction of the concrete member

The crack spacing $l_{cr,m}$ is described as suggested in Bazant and Wahab [6] in Equation 2.9. Krips [2] estimated the value of k_c as 1.28. s_{cr} is the vertical height of the major crack part.

$$l_{cr,m} = \frac{s_{cr}}{k_c} \quad (2.9)$$

The major cracks then develop to form critical inclined cracks. Using Equation 2.9 and simplifying the expression, the crack width w_b is estimated as shown in Equation 2.10.

$$w_b = l_{cr,m} \varepsilon_s \quad (2.10)$$

Considering the cross-sectional equilibrium the vertical height s_{cr} is calculated as given in Equation 2.11

$$s_{cr} = \left[1 + \rho_s n_e - \sqrt{2\rho_s n_e + (\rho_s n_e)^2} \right] d \quad (2.11)$$

2.3.3. SIMPLIFIED SHEAR FORCE-DISPLACEMENT RELATIONSHIP

In this shear force-displacement relationship, shear stress transfer due to aggregate interlock is the most important. This is calculated by using the parameters of shear crack displacement and the crack width. The shear stress expression for aggregate interlock is $\tau_{ai}(\Delta, w)$ (Equation 2.13) which is integrated along the vertical crack to obtain the shear force as shown in Equation 2.12.

$$V_{ai} = \int_0^{s_{cr}} \tau_{ai}[\Delta, w(s)] b ds \quad (2.12)$$

In the above Equation 2.12, the analytical shear stress expression is proposed by Walraven [7].

$$\tau_{ai} = \sigma_{pu} \{ \mu A_x[\Delta, w(s)] + A_y[\Delta, w(s)] \} \quad (2.13)$$

The complex form of Equation 2.12 can be modified using simplified crack profile and then applying Walraven's aggregate interlock expression. Substituting Equation 2.13 and using expression for $\sigma_{pu} = 6.39 f_c^{0.56}$, Equation 2.12 takes form of Equation 2.14

$$V_{ai} = 6.39 f_c^{0.56} b s_{cr} v_{ai} \quad (2.14)$$

where,

$$v_{ai} = \int_{w_t}^{w_b} [\mu A_x(\Delta, w) + A_y(\Delta, w)] dw$$

A_x and A_y are the projected areas of the crack surface for a unit crack length as described by Walraven. These are functions of tangential and normal displacement (Δ, w) of the crack faces. From the reference document for this method, it can be observed that this expression of shear force can be further simplified as Equation 2.15.

$$V_{ai} = f_c^{0.56} s_{cr} b \frac{0.03}{w_b - 0.01} (-978\Delta^2 + 85\Delta - 0.27) \quad (2.15)$$

When the results obtained by using Equation 2.15 are compared with those of Equation 2.14, a striking similarity is observed in the results as described in the reference document [2].

2.3.4. DETERMINATION OF THE CRITICAL SHEAR DISPLACEMENT Δ_{cr}

The total shear force transferred along the crack is expressed by a final expression shown in Equation 3.3.4.

$$V = V_{ai} + V_c + V_d \quad (2.16)$$

Where, V_{ai} can be calculated using Equation 2.14 or the simplified version Equation 2.15. The shear force in the compression zone is calculated using Morsch's [8] approach. Here, the residual tensile stresses are neglected and a linear stress distribution is assumed as given by Equation 2.17.

$$V_c = \frac{2}{3} \frac{z_c}{z} V = \frac{d - s_{cr}}{d + 0.5s_{cr}} V \quad (2.17)$$

Baumann and Rusch [9] proposed an expression for the shear force transferred by dowel action (Equation 2.18), considering that the maximum value of dowel force is obtained when Δ_{cr} is reached.

$$V_d = 1.64 b_n \phi \sqrt[3]{f_c} \quad (2.18)$$

For calculating the value of V_{ai} , crack width at the bottom part of the flexural crack is needed which is obtained by Equation 2.19

$$w_b = \frac{M}{z A_s E_s} l_{cr,m} \quad (2.19)$$

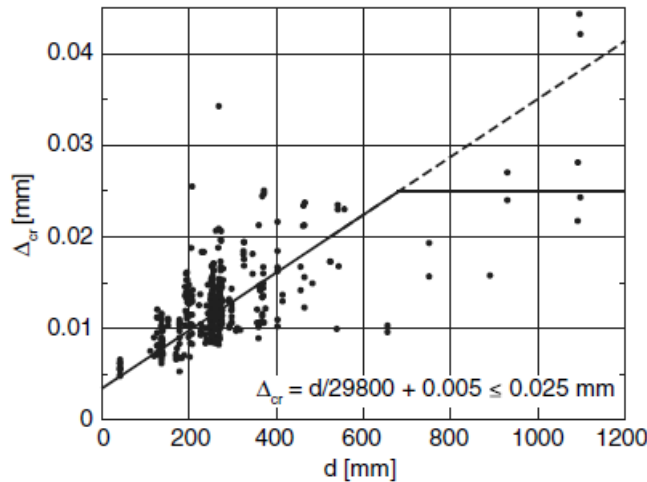


Figure 2.4: Calculated critical shear displacement Δ_{cr} against the effective depth d [2]

The graph in Figure 2.4 clearly shows that Δ_{cr} values are greatly influenced by the depth of beams. But these Δ_{cr} values are comparable in the lower range of d values. Therefore, an expression for Δ_{cr} is suggested

in the reference document as given in Equation 2.20.

$$\Delta_{cr} = \frac{d}{29800} + 0.005 \leq 0.025 \text{ mm} \quad (2.20)$$

Moreover, Yang [3] proposed that the rebar diameter influences the Δ_{cr} values as well. For instance, under the same dowel force, lower dowel displacement is obtained due to a larger rebar diameter because of higher flexural stiffness. Hence, the Equation 2.20 was changed to account for the rebar diameter for calculating Δ_{cr} as given in Equation 2.21.

$$\Delta_{cr} = \frac{25d}{30610\phi} + 0.0022 \leq 0.025 \text{ mm} \quad (2.21)$$

2.3.5. EVALUATION OF SHEAR CAPACITY BASED ON CRITICAL SHEAR DISPLACEMENT

To get a clear idea for calculating the shear capacity using CSDM a pictorial representation is shown in Figure 2.5.

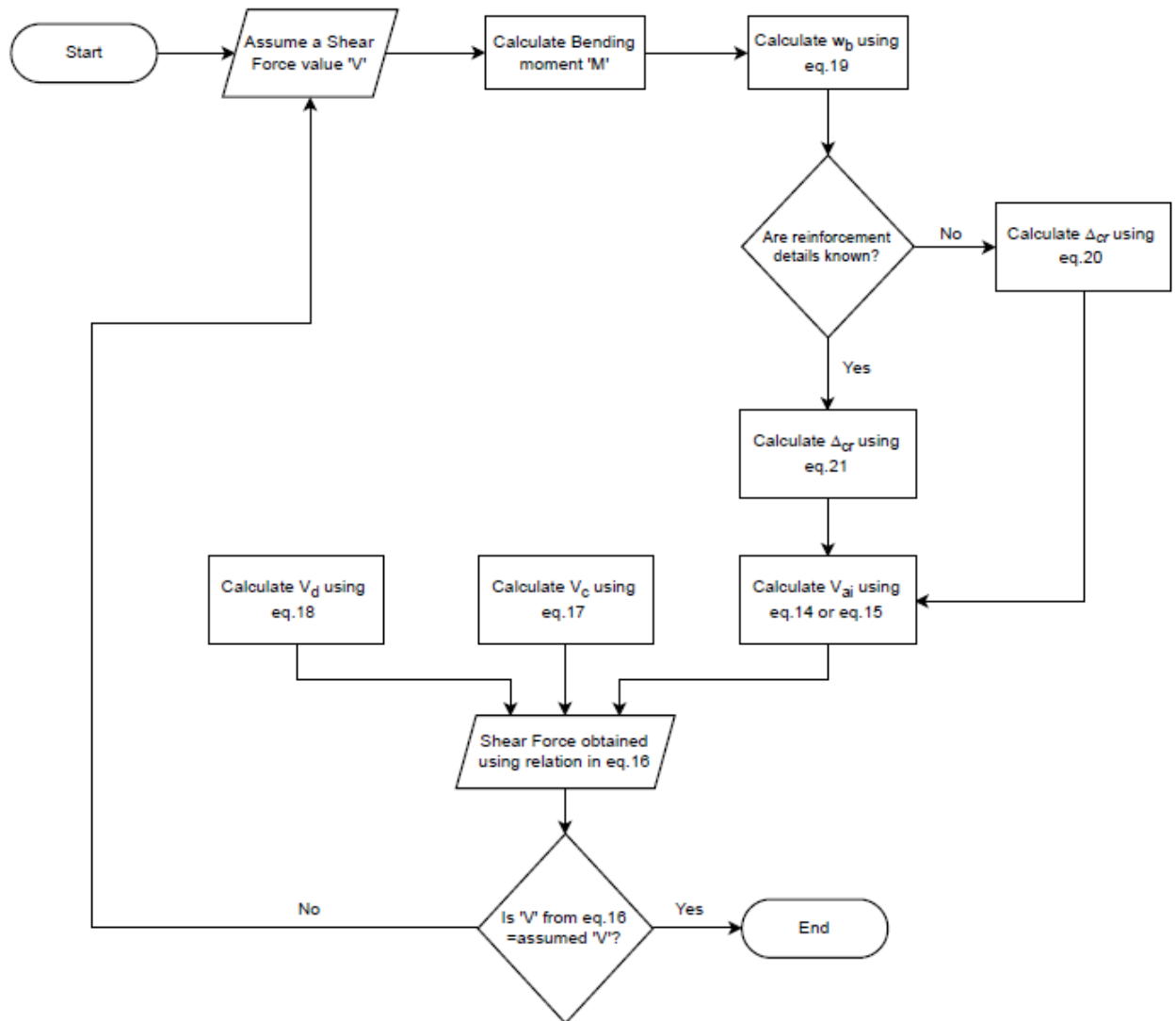


Figure 2.5: Flowchart for finding the shear capacity

2.3.6. SLAB FACTOR: INFLUENCE OF SPECIMEN WIDTH

In his research, Yang [3] discusses the influence of specimen width on the shear capacity of a concrete member. The observations of the research show that the shear capacity of a concrete member is greatly affected by the width-depth ratio. In case of a slab, the width-depth ratio is larger than that of a beam and so it has a greater shear capacity than a concrete beam. Yang also compares the results with other researchers, like Conforti, Minelli [3] with their respective experimental results on shallow specimens.

To explain this behaviour, a one way homogeneous slab was considered. Any strip of the slab in the transverse (width) direction should exhibit a similar behaviour as per the theory since the boundary conditions and structural performance are the same for all. Therefore, the shear capacity of any strip in the span direction should be approximately the same as compared to the entire slab specimen.

Furthermore, there is also a substantial difference in the deformation of the slab specimen along the transverse direction, as compared to the beam element. In a beam, the crack at a local weak cross section propagates through the entire width. Whereas, in case of a slab, the crack profile along the span direction doesn't spread homogeneously throughout the width, rather it spreads by connecting all the local weak spots along a critical zone. It finally develops into a final crack pattern through the width. There is a random distribution of weak spots along the transverse direction as well. These weak spots are assumed to form a wavy shape of the cracks for ease of calculation. This shape influences the shear stress transferred through the aggregate interlock component in following two ways,

- The shear force transferred through aggregate interlock increases (Equation 2.22) as the wavy crack profile subsequently increases the length of the crack profile.

$$V'_{ai} = \frac{b_{cr}}{b} V_{ai} \quad (2.22)$$

where, b_{cr} is the real length of the critical crack.

- A shift of the crack position occurs in the longitudinal direction (thick crack shown in Figure 2.6) because of the wavy crack profile. This also means that a single crack does not propagate entirely through the transverse direction. This shift can be observed between the two red lines in Figure 2.6. Dowel action is a plastic mechanism. Until the stress in the reinforcement does not reach its yield strength, full capacity of the slab will not be utilized. Vertical displacement of the cracked concrete (part c in Figure 2.3) is kept in causing this dowel action phenomenon. Once the vertical displacement in the bottom part of the slab reaches Δ_{cr} value throughout the width of slab, then the dowel crack develops. Therefore, rotation capacity increases and also the critical shear displacement Δ_{cr} value.

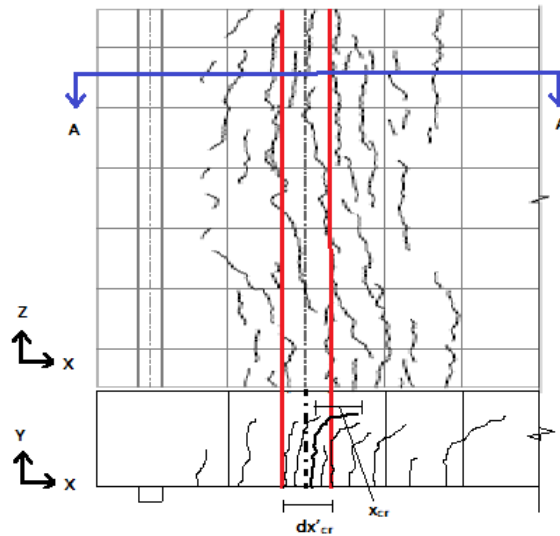


Figure 2.6: Crack distribution along section A-A showing average crack variation (dx'_{cr}) and crack length in longitudinal direction (x_{cr})

$$\Delta' = \theta(x_{cr} + dx'_{cr}) = \Delta_{cr} \left(1 + \frac{dx'_{cr}}{x_{cr}}\right) \quad (2.23)$$

where,

x_{cr} : length of the inclined crack in longitudinal direction,
 dx'_{cr} : average variation of the transverse crack profile.

Both the above parameters greatly depend on the random crack profile in the span direction. In other words, the crack profile can be assumed as a triangular wave by considering the simple geometry of the wave. This consideration explains the crack profile depending on its amplitude and wave length.

Refer Figure 2.7 in which a simply supported slab is shown and a strip in the transverse direction is considered to explain the slab factor.

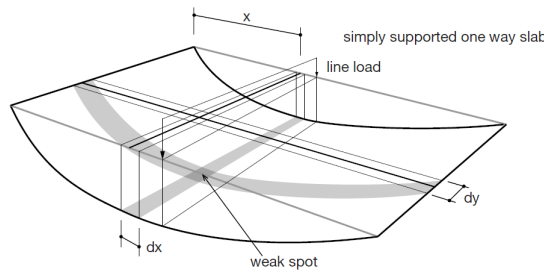


Figure 2.7: Simplified model of slab to understand the slab factor ([3])

AMPLITUDE

The variation of the crack profile must be in the limits of the maximum crack spacing, created due to the bond between concrete and reinforcement. Thus, the amplitude (A_p) can be defined as the average crack spacing $l_{cr} = \Psi_s l_t$, where $\Psi_s = 1.5$ and l_t can be defined by Equation 2.24.

$$l_t = \frac{f_{ctm}\phi}{4\tau_{bm}\rho_{eff}} \quad (2.24)$$

where,

f_{ctm} : Mean tensile strength of concrete
 ϕ : Diameter of rebar
 τ_{bm} : Friction between concrete and steel reinforcement
 ρ_{eff} : Effective reinforcement ratio, $\rho_{eff} = A_s/A_{c,eff}$

WAVE LENGTH

To explain this phenomenon the influence area of the crack is studied. Outside this influence area a crack developed in the adjacent zone will have no effect on the nature of the crack in consideration. A new peak can be formed in this new adjacent zone and the distance between the two peaks is equal to half of the average wave length of the curve.

The final expression for calculating the wave length is given by 2.25. For further information on the calculation of the wave length refer Yang's research [3].

$$l_w = \pi \sqrt[4]{\frac{4EI_x}{k_w}} = \pi \sqrt[4]{\frac{4x^2(l-x)^2 dx}{3l}} \quad (2.25)$$

where,

dx : width of the transverse strip, also the average crack spacing l_{cr}

Thus, the average wave length of the crack profile will be equal to $2l_w$.

Estimation of these two factors assist in the calculation of the crack length and the critical shear displacement. By calculating values of amplitude and wave length for the given specimen, the actual crack length can be calculated by Equation 2.26.

$$b_{cr} = b \frac{T}{\sqrt{T^2 + A_p^2}} \quad (2.26)$$

Moreover, for the vertical shear displacement, it can be calculated using Equation 2.23, where, the additional length is $dx'_{cr} = A_p/2$. In the reference document [3], details of the numerically proven data can be checked for further clarification. In general, for slabs subjected to multiple point loads or line loads, a good estimation can be made according to the described phenomenon. An average increase of 18.2% (slab factor = 1.182) is observed which is a quite stable estimation, also proven in [3]. Furthermore, as an engineering approach, a rough width factor of $\gamma_w = 1.1$ can be assumed for a more accurate evaluation of the shear capacity of concrete slabs.

A MATLAB code was developed for the ease of calculation of shear capacity by Critical Shear Displacement Theory which is attached in the appendix A. However, the code doesn't consider the slab factor since it was developed considering concrete beam elements. Thus, the slab factor has to be considered separately for calculating the shear capacity of concrete slab by CSDM.

In the procedure prescribed by Eurocode2, number of assumptions are made to calculate the shear capacity of a concrete member. This is evident from the use of various factors in the formulae leading to the shear capacity of the concrete member. Also, the effect of concrete in compressive zone is neglected while calculating the shear capacity. In the critical shear crack theory, contribution of the concrete in compressive zone is taken into consideration to improve the accuracy of results. The micro cracks in the shear band subsequently lead to the critical inclined crack, thus improving the shear capacity of the concrete member. This can also be explained by the strut and tie phenomenon. Finally, in the critical shear displacement theory, effect of the vertical displacement caused by cracking is also taken into consideration along-with the effect of concrete in compressive zone. In case of a concrete slab, the vertical displacement caused by cracking of the secondary diagonal crack (Figure 2.3), leading from a vertical crack, increases the shear capacity substantially. Moreover, a cracking pattern is obtained in the transverse direction along all the weak spots that enhances the aggregate interlocking effect along the cracked planes. For example, in case of concrete beams the maximum vertical shear displacement is achieved as soon as the entire cross-section cracks along the width of the beam. Whereas, in case of concrete slab, width of the member is much larger as compared to a concrete beam, thus a greater force is required to induce cracks throughout the width of the slabs. Moreover, the reinforcement quantity is substantially higher in slabs. A higher shear force is needed to achieve necessary crack width throughout the width in order to activate yielding of reinforcement. As the dowel action is a plastic phenomenon, reinforcement in the slab has to reach its plastic state for full effect on shear transfer by dowel action. This greater shear force is thus responsible for the maximum shear displacement. The following research question is proposed considering the knowledge from the literature study performed.

How can the shear capacity of a composite concrete slab be calculated?

An attempt is made to calculate the shear capacity of a composite concrete slab specimen by performing an extensive analytical study considering the three shear models described in the literature section. The shear models propose theories for homogeneous slabs but in this case some alterations and assumptions are made to understand the response of composite concrete slab specimens. To start with the comparison, two separate homogeneous slab specimens are considered having material properties of substrate concrete layer (NSC) and overlay concrete layer (HSC). Shear resistance of these homogeneous slabs is calculated using the propositions of the shear models. Furthermore the shear resistance obtained from the slab is assumed to give an upper and lower limit value for the actual composite slab specimen. An average is calculated considering these upper and lower bound limiting values and a direct comparison is done among the different shear models and further findings from an experiment performed by *Dr. Randl* are considered as basis for the comparison of analytical results. Finally a validation is performed by comparing the results to a numerical model. Validation of the shear stress values at the interface of the two concrete layers is also carried out with a numerical analysis performed using ATENA finite element software.

3

Case Study

The use of high strength concrete has been widely acclaimed in the form of an overlay over the existing concrete structures. Many experiments have been carried out to understand the behaviour of the composite concrete beams and slabs to understand the shear and bending behaviour. One such experiment was carried out by Dr. Randl on a concrete slab with a concrete topping. The concrete topping/overlay was cast over the specimen after the reinforced concrete (RC) slab had started hardening. Details about this case study and findings of the experiment are discussed in this chapter.

3.1. PREPARATION OF THE TEST SPECIMENS

To increase the strength of a RC bridge, a high strength concrete overlay is applied and the results of these experiments are documented in Dr. Randl [4]. He conducted this research using 10 concrete slab specimens (360 × 100 × 24cm) in the form of test plates which were formed as an in-house service by the construction company Strabag. On the basis of detailed planning (load capacity, reinforcement and measurements) of the test plates, a smooth production process was achieved.

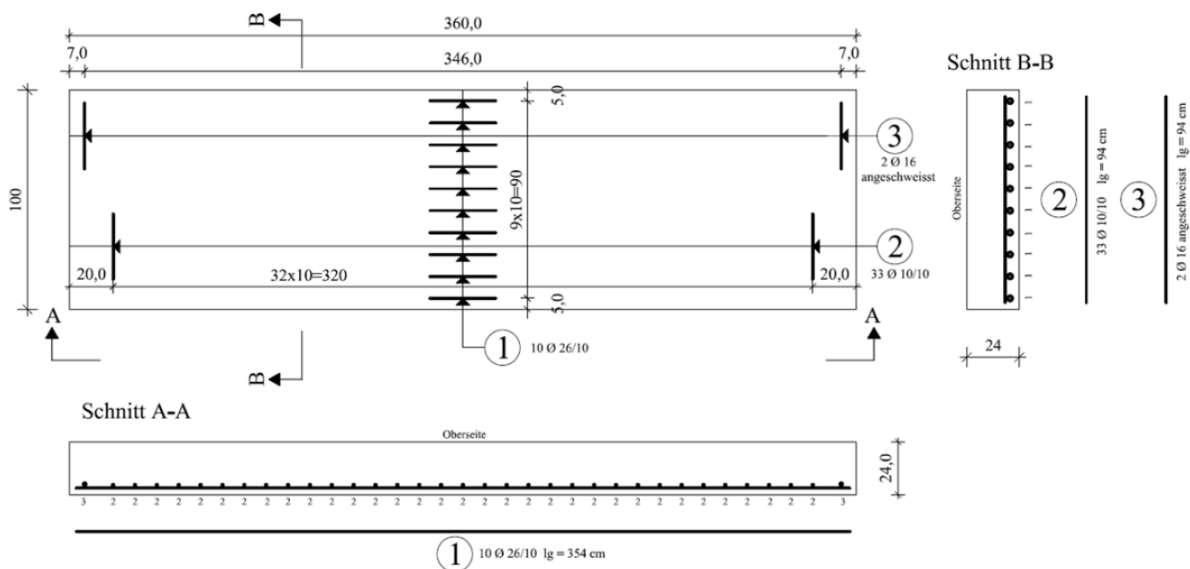


Figure 3.1: Reinforcement layout of the test specimens [4]

A 24cm thick base plates were provided with strong bending reinforcement, to avoid a premature bending failure during the four-point bending test. The goal was to transfer the failure load such that the point with highest shear stress is recognized. The experiment included 3 test plates finished with Normal Strength Concrete (NSC) and the remaining 7 plates were applied a High Strength Concrete (HSC) topping.



Figure 3.2: Preparation of the test plates [4]

After the curing of almost 3 weeks, the surface of the test specimens was roughened by means of high-pressure water jet (about 2000 bar). The roughness was fabricated as per the Eurocode 2 classification: smooth, rough and toothed. The measurement of the surface roughness was carried out by the sand surface method according to Kaufmann and also by the creation of digital surface models. Later, the specimens were transported to the storage area of the FH-Baulabors where the concreting of 6 cm thick topping was done.



Figure 3.3: Surface treatment and concreting at construction yard [4]

Corresponding to the large body test plates, small body specimens were also developed to examine the surface properties in more detail.

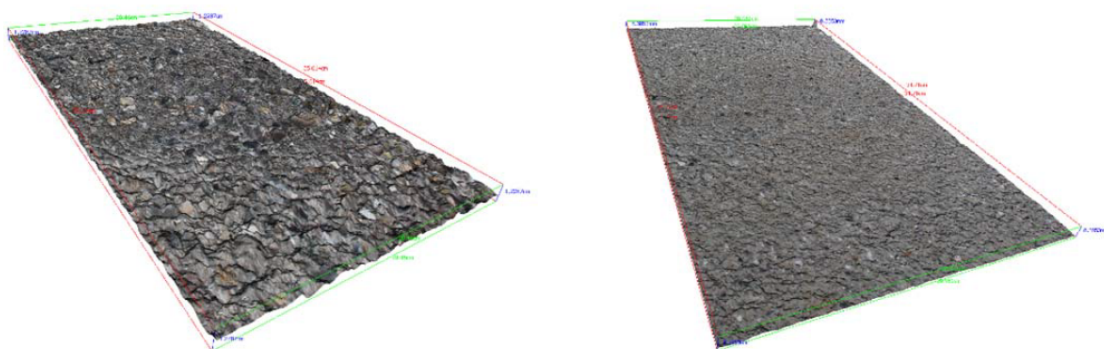


Figure 3.4: Digital surface models of a rough(left) and smooth(right) specimen section [4]

Table 3.1 gives an overview of the test specimens with the variations in surface roughness, layer of concrete and the load peaks that were reached.

Table 3.1: Specimen details and respective Load Maxima [4]

No.	Roughness [mm]	Topping	1.LM [kN]	2.LM [kN]	3.LM [kN]
1	1.6	NSC	902.4	917.7	950.9
2	3.0	HSC	951.3	993.7	1056.8
3	3.0	NSC	914.1	878.8	×
4	0.8	NSC	942.6	928.9	×
5	1.5	HSC	951.9	967.3	×
6	1.7	HSC	896.7	×	×
7	0.8	HSC	1014.9	878.6	×
8	0.8	HSC	947.2	1003.1	1438.0

3.2. IMPLEMENTATION OF FOUR-POINT BENDING TEST

This section mainly describes the implementation of the four-point bending test, carried out for the determination of the structural behaviour of the test plates. The test setup is shown in the Figure 3.5.

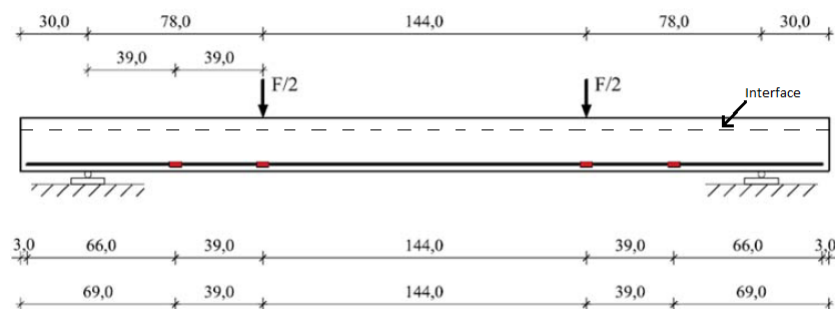


Figure 3.5: Test setup for 4-point bending test [4] [all dimensions are in cm]

The test plates were loaded using a hydraulic press. The loading was applied static-path-monotonically with about 1.0 mm/min (piston stroke). The main condition of the experiment was to achieve highest possible shear stress.



Figure 3.6: Actual test setup in the laboratory [4]

3.3. COMPARISON OF SHEAR MODELS BASED ON THE INPUT PARAMETERS FROM THE CASE STUDY

Three shear models are described in chapter 2 which are dependent on different parameters to calculate the shear capacity of a concrete member. These models are compared in this section to have a basis for further development of a numerical model required for a composite concrete slab specimen. The procedure for the comparison and the necessary checks have been described hereafter.

3.3.1. PROCEDURE FOR COMPARISON OF THE SHEAR MODELS

The following section explains the difference between the aforementioned shear models in detail, and the steps involved in the comparison of these models. The input data used for the comparison of the models is taken from the report of Dr. Randl [4]. The model of the case study under consideration is a slab with composite cross-section having two layers with different concrete compressive strengths. The bottom layer is called the substrate and the top layer is overlay layer.

An estimation of the shear resistance for a composite concrete slab has to be performed. There are no guidelines available for modeling such a composite slab specimen. Hence, to start with the modeling it is assumed that, the slab is made of only one homogeneous material at a time, out of the two different compressive strengths. Thus, a range of shear resistances will be obtained for two separate homogeneous concrete slabs. These two values are assumed to be the limiting cases for the composite concrete slab specimen. That means shear capacity of the composite concrete slab should lie in between the shear capacities of these two homogeneous slabs. Slab made of low strength concrete is assumed to have shear capacity in the lower limit of the aforementioned shear range. Whereas, the one with high strength concrete should have the upper limit values for shear capacity.

For the shear resistance range estimation, as described before, two different homogeneous concrete slabs with exact same dimensions, as in the experiment, are considered as shown in Figure 3.7. This will also help in the comparison of the shear models. The first slab in the figure is the composite slab as in the case study experiment, the second slab has the substrate concrete layer material properties (normal strength concrete) for the analysis while the third slab has the overlay concrete material properties (high strength concrete). The loading and boundary conditions in all the cases are identical as in the actual experiment for the respective slab specimens. Thus, an identical nature of shear force at a critical cross section is ensured. Next step is to compare the results obtained from these homogeneous slab specimens to conclude the choice of a shear model which best describes the shear behaviour in a composite concrete slab. Table 3.2 gives the material properties of the actual experiment carried out by Dr. Randl [4]. The table gives the values of the compressive strength of concrete cubes cast with the same material as used in the experiments. To use these values in the computation of shear resistance calculation, (as per the guidelines of the shear models) they have to be converted into cylindrical concrete compressive strength. For this purpose a factor of 0.8155 is assumed which is multiplied with the $f_{c,cube}$ values, (as per the observations in Eurocode 2 NEN-EN 1992-1-1 (Figure B.2 of appendix B)) to obtain the compressive strength of concrete cylinder $f_{c,cyl}$. Henceforth, $f_{c,cyl}$ is considered as the concrete compressive strength used for all the calculations.

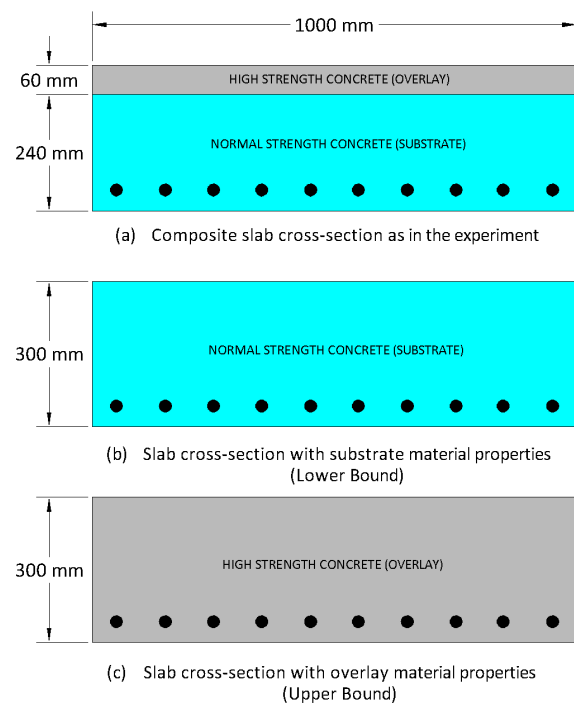


Figure 3.7: Slab cross-sections (a) Composite slab (b) with substrate concrete properties (lower bound) (c) with overlay concrete properties (upper bound)

Table 3.2: Material properties used in experiment

Slab no.	Layers	$f_{c,cube}$ [MPa]	Modulus of Elasticity [MPa]
1	Substrate	62.09	28390
	Overlay	50.47	25470
2	Substrate	61.80	28640
	Overlay	88.40	36510
3	Substrate	61.96	28390
	Overlay	49.79	25470
4	Substrate	61.74	28390
	Overlay	47.30	25470
5	Substrate	59.48	28640
	Overlay	97.59	36510
6	Substrate	49.01	28640
	Overlay	101.79	37450
7	Substrate	66.86	28640
	Overlay	93.27	36510
8	Substrate	57.28	28990
	Overlay	98.79	37450

3.3.2. SHEAR RESISTANCE CALCULATION USING EUROCODE

A sample calculation is shown below, using the input data of slab specimen 8 based on relations in section 2.2. Detailed calculations are given in appendix B in Figure B.3.

For slab with homogeneous material properties of substrate,

$$b = 1000 \text{ mm},$$

$$h = 300 \text{ mm},$$

$$d = 257 \text{ mm} \quad (d = h - \text{cover} - \frac{\phi}{2}),$$

$$f_{c,cube} = 57.28 \text{ MPa},$$

$$f_{c,cyl.} = 57.28 \times 0.8155 = 46.71 \text{ MPa}$$

$$k = 1 + \sqrt{\frac{200}{257}} = 1.882$$

$$v_{min} = 0.035 \times (1.882)^{3/2} \times (46.71)^{1/2} = 0.618 \text{ MPa} \quad (3.1)$$

$$V_{Rd,c,min} = (0.618 + 0.15 \times 0.00) \times 1000 \times 257 = 158.75 \text{ kN}$$

$$V_{Rd,c,LB} = [0.12 \times 1.882 \times (100 \times 0.02 \times 46.71)^{1/3} + 0.15 \times 0.00] \times 1000 \times 257 = 247.04 \text{ kN}$$

For slab with homogeneous material properties of overlay,

$$b = 1000 \text{ mm},$$

$$h = 300 \text{ mm},$$

$$d = 257 \text{ mm} \quad (d = h - \text{cover} - \frac{\phi}{2}),$$

$$f_{c,cube} = 98.79 \text{ MPa},$$

$$f_{c,cyl.} = 98.79 \times 0.8155 = 80.56 \text{ MPa}$$

$$k = 1 + \sqrt{\frac{200}{257}} = 1.882$$

$$v_{min} = 0.035 \times (1.882)^{3/2} \times (80.56)^{1/2} = 0.811 \text{ MPa} \quad (3.2)$$

$$V_{Rd,c,min} = (0.811 + 0.15 \times 0.00) \times 1000 \times 257 = 208.48 \text{ kN}$$

$$V_{Rd,c,UB} = [0.12 \times 1.882 \times (100 \times 0.02 \times 80.56)^{1/3} + 0.15 \times 0.00] \times 1000 \times 257 = 304.53 \text{ kN}$$

Thus, from Equations 3.1 and 3.2 for slab 8, the lower bound limit for shear force capacity is 247.04 kN while the upper bound limit is 304.53 kN. An average of these values is compared with the actual experimental shear force value.

Table 3.3: Variation of eurocode model with experimental results (Slab 8)

Slab no.	Lower Bound shear force ($V_{Rd,c,LB}$) [kN]	Upper Bound shear force ($V_{Rd,c,UB}$) [kN]	Average shear force (V_{EC}) [kN]	Shear Force (experimental) (V_{exp}) [kN]	V_{EC}/V_{exp}
8	247.04	304.53	275.79	473.60	0.58

Table 3.3 shows a very large variation of shear force results obtained from calculations based on Eurocode model and the experimental results. This significant variation is clearly not desirable. Rest of the data from remaining slabs is tabulated in Table 3.4 with their respective experimental results.

Table 3.4: Variation of eurocode model with experimental results (All slab specimens)

Slab no.	Lower Bound shear force ($V_{Rd,c,LB}$) [kN]	Upper Bound shear force ($V_{Rd,c,UB}$) [kN]	Average shear force (V_{EC}) [kN]	Shear Force (experimental) (V_{exp}) [kN]	V_{EC}/V_{exp}
1	234.62	255.11	244.87	451.20	0.54
2	254.64	292.20	273.42	475.65	0.57
3	233.31	254.90	244.10	457.05	0.53
4	228.37	254.54	241.45	471.30	0.51
5	250.80	303.16	276.98	475.95	0.58
6	231.78	307.91	269.85	448.35	0.60
7	262.64	298.11	280.37	507.45	0.55
8	247.04	304.53	275.79	473.60	0.58
Mean Value					0.56

This variation of shear force calculated using Eurocode guidelines has a COV of 4.99 % which can be seen in Figure 5.1.

3.3.3. SHEAR RESISTANCE CALCULATION USING CRITICAL SHEAR CRACK THEORY

A sample calculation is shown, using the input data of slab specimen 8 based on relations in section 2.2. Detailed calculations are given in appendix B in Figure B.4.

For slab with homogeneous material properties of substrate,

$$b = 1000 \text{ mm},$$

$$d = 257 \text{ mm},$$

$$d_g = 32 \text{ mm},$$

$$f_{c,cyl.} = 46.71 \text{ MPa},$$

$$E_s = 210000 \text{ MPa},$$

$$E_c = 28990 \text{ MPa},$$

$$M = V \times a,$$

$$M = 473.60 \times 0.780 = 369.41 \text{ kN-m}$$

$$c = 257 \times 0.02 \times \frac{210000}{28990} \times \left(\sqrt{1 + \frac{2 \times 28990}{0.02 \times 210000}} - 1 \right) = 114.98 \text{ mm}$$

$$\varepsilon = \frac{369.41 \times 10^6}{1000 \times 257 \times 0.02 \times 210000 \times (257 - 114.98/3)} \times \frac{0.6 \times 257 - 114.98}{257 - 114.98} = 3.46 \times 10^{-4} \quad (3.3)$$

$$V_{R,LB} = \frac{1}{6} \times \frac{2 \times 1000 \times 257 \times \sqrt{46.71}}{1 + 120 \times \frac{3.46 \times 10^{-4} \times 257}{16 + 32}} = 479.07 \text{ kN}$$

For slab with homogeneous material properties of overlay,

$$b = 1000 \text{ mm},$$

$$d = 257 \text{ mm},$$

$$\begin{aligned}
 d_g &= 32 \text{ mm}, \\
 f_{c,cyl} &= 80.56 \text{ MPa}, \\
 E_s &= 210000 \text{ MPa}, \\
 E_c &= 37450 \text{ Mpa},
 \end{aligned}$$

$$\begin{aligned}
 M &= 473.60 \times 0.780 = 369.41 \text{ kN-m} \\
 c &= 257 \times 0.02 \times \frac{210000}{37450} \times \left(\sqrt{1 + \frac{2 \times 37450}{0.02 \times 210000}} - 1 \right) = 104.74 \text{ mm} \\
 \varepsilon &= \frac{369.41 \times 10^6}{1000 \times 257 \times 0.02 \times 210000 \times (257 - 104.74/3)} \times \frac{0.6 \times 257 - 104.74}{257 - 104.74} = 4 \times 10^{-4} \quad (3.4) \\
 V_{R,UB} &= \frac{1}{6} \times \frac{2 \times 1000 \times 257 \times \sqrt{80.56}}{1 + 120 \times \frac{4 \times 10^{-4} \times 257}{16 + 32}} = 611.57 \text{ kN}
 \end{aligned}$$

Thus, from Equations 3.3 and 3.4 for slab 8, the lower bound limit for shear force capacity is 479.07 kN while the upper bound limit is 611.57 kN. An average of these values is compared with the actual experimental shear force value.

Table 3.5: Variation of CSCT model with experimental results (Slab 8)

Slab no.	Lower Bound shear force ($V_{R,LB}$) [kN]	Upper Bound shear force ($V_{R,UB}$) [kN]	Average shear force (V_{CSCT}) [kN]	Shear Force (experimental) (V_{exp}) [kN]	V_{CSCT}/V_{exp}
8	479.07	611.57	545.32	473.60	1.15

Table 3.5 shows a small variation of the shear force capacity, calculated using CSCT, to the experimental results. Moreover, the variations of rest of the specimens is tabulated below in Table 3.6.

Table 3.6: Variation of CSCT model with experimental results (All slab specimens)

Slab no.	Lower Bound shear force ($V_{R,LB}$) [kN]	Upper Bound shear force ($V_{R,UB}$) [kN]	Average shear force (V_{CSCT}) [kN]	Shear Force (experimental) (V_{exp}) [kN]	V_{CSCT}/V_{exp}
1	461.27	504.39	482.83	451.20	1.07
2	497.99	579.46	538.72	475.65	1.13
3	457.20	502.74	479.97	457.05	1.05
4	443.37	499.13	471.25	471.30	1.00
5	488.50	608.75	548.63	475.95	1.15
6	448.13	627.64	537.89	448.35	1.20
7	511.78	587.22	549.50	507.45	1.08
8	479.07	611.57	545.32	473.60	1.15
Mean Value					1.10

This small variation due to shear force calculated using critical shear crack theory (CSCT) has a COV of 5.54 % as also can be seen in Figure 5.1.

3.3.4. SHEAR RESISTANCE CALCULATION USING CRITICAL SHEAR DISPLACEMENT THEORY

A detailed MATLAB code developed by Yang is attached in the appendix A. Through this code, the relations in section 3.8 are used to compute the shear force capacity of a concrete member subjected to similar loading conditions as in the experiment.

In the code, the main function depends on a number of parameters which have to be defined as per the experimental conditions. (*The symbols shown hereafter in parentheses are used in the MATLAB code for the*

parameters as described further) These parameters are the M/Vd ratio (mvd) of the concrete beam, concrete compressive strength (f_c), effective depth of the beam (d), width of the beam (bw), maximum aggregate size (da), reinforcement ratio (ρ) and the reinforcement configuration (Re), where Re is expressed as a two column matrix. The first column is the number of rebar while the second column is the diameter of the rebar. For example, if the beam consists of 3 steel bars of 20 mm diameter then the Re matrix will be [3, 20].

In Table 3.7, the input parameters that are used to obtain the required results and the respective outputs are tabulated.

Table 3.7: Input parameters and output for lower and upper bound limits using CSDT method (Slab 8)

Description	Symbol	Unit	Lower bound (substrate properties)	Upper bound (overlay properties)
INPUT PARAMETERS				
Aspect ratio	M/Vd	(-)	3.035	3.035
Maximum aggregate size	d_g	mm	32	32
Effective depth of the beam	d_{eff}	mm	257	257
Width of the beam	b	mm	1000	1000
Concrete compressive strength	f_c	MPa	46.71	80.56
Reinforcement ratio	ρ	(-)	0.02066	0.02066
Reinforcement configuration	Re	(-)	[10 26]	[10 26]
OUTPUT				
Maximum shear displacement	Δ	mm	0.0103	0.0103
Average crack spacing of major cracks	s_{cr}	mm	116.95	124.64
Major crack height	h_{cr}	mm	147.70	159.53
Shear force due to aggregate interlock	V_{ai}	kN	154.32	167.64
Shear force due to uncracked concrete	V_c	kN	127.37	122.98
Shear force due to dowel action	V_d	kN	112.19	134.30
Total shear force	V	kN	393.88	424.92

The results obtained are tabulated below in Table 3.8 for clear understanding. Detailed calculations are given in appendix B in Figure B.5.

Table 3.8: Variation of CSDT model with experimental results (Slab 8)

Slab no.	Lower bound shear force ($V_{i,LB}$) [kN]	Upper bound shear force ($V_{i,UB}$) [kN]	Average shear force excluding SF (V_{ESF}) [kN]	Shear Force (experimental) (V_{exp}) [kN]	V_{ESF}/V_{exp}
8	393.88	424.92	409.40	473.60	0.86

The variation (V_{ESF}/V_{exp}) obtained by this method is still not satisfactory. This may be because the code developed by Yang is for a concrete beam and not for a concrete slab. To refine the results further, the slab factor mentioned in section 2.3.6 is implemented to estimate the results as close to that of a concrete slab as possible.

This slab factor can be incorporated in two ways. One way is by calculating the actual slab factor depending on the amplitude and wave length of the crack profile considering the wave profile to be a wave function. Second way is to use the slab factor estimation as described in section 2.3.6. The slab factors from both the methods are incorporated in the results obtained from CSDT as following.

METHOD 1: ACTUAL CALCULATION OF SLAB FACTOR (SF_{act})

The actual slab factor (SF_{act}) is calculated by using the Equations 2.22 - 2.26 from section 2.3.6. This slab factor comprises of two parameters; Amplitude (A) and Wavelength (T) which enhances the shear capacity in case of a concrete slab. In the calculation of amplitude, the term ρ_{eff} is different from the actual reinforcement ratio. It is the reinforcement ratio near the tension zone which is the effective region in cracking of material. The expression for $\rho_{eff} = A_s/bh_{c,eff}$ is valid, where $h_{c,eff} = 2.5(h - d)$. Therefore, following calculations can be carried out.

$$\rho_{eff} = \rho \frac{d}{h_{c,eff}} = 0.02066 \times \frac{257}{2.5 \times (300 - 257)}$$

$$\rho_{eff} = 0.04939$$

$$Amplitude (A) = l_{cr} = \Psi l_t = 1.5 \times \frac{26}{4 \times 2 \times 0.04939} \quad (3.5)$$

$$Amplitude (A) = 98.70 \text{ mm}$$

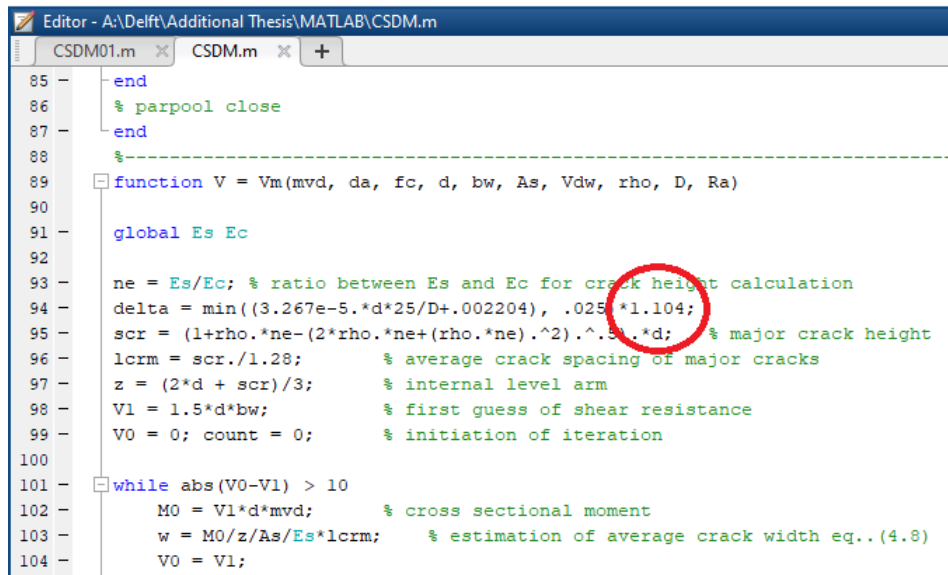
This is assuming the bond strength equal to twice the value of the tensile strength $\tau_{bm} = 2 \times f_{ctm}$. The amplitude will be same for all slab specimens. But as far as the wave length is considered, it will change for every slab specimen depending on the critical moment values which will be discussed further in section 3.4. A sample calculation of the wave length is shown below.

$$Wavelength (T) = 2 \times l_w = 2 \times \pi \sqrt{\frac{4 \times 304.72^2 \times (3600 - 304.72)^2 \times 98.70}{3 \times 3600}} \quad (3.6)$$

$$Wavelength (T) = 2753.06 \text{ mm}$$

In such a manner, all the wave lengths are calculated for individual specimens. It is observed that there is no substantial difference between the wave lengths. Moreover, the values of these wave lengths are significantly high which reduces its effect on the shear strength.

The factor $f = (1 + \frac{dx'_{cr}}{x_{cr}})$ in Equation 2.23 is calculated with an average value of 1.104 considering all 8 slab specimens. This factor 'f' is incorporated in the MATLAB code (while obtaining the Δ value as can be seen in Figure 3.8) to obtain new values of shear forces transferred by all the mechanisms described in section 2.3.2.



```

85 - end
86 - % parpool close
87 - end
88 - %-----
89 - function V = Vm(mvd, da, fc, d, bw, As, Vdw, rho, D, Ra)
90 -
91 - global Es Ec
92 -
93 - ne = Es/Ec; % ratio between Es and Ec for crack height calculation
94 - delta = min((3.267e-5.*d*25/D+.002204), .025*1.104);
95 - scr = (1+rho.*ne-(2*rho.*ne+(rho.*ne).^2).^0.5).^2.*d; % major crack height
96 - lcrm = scr./1.28; % average crack spacing of major cracks
97 - z = (2*d + scr)/3; % internal level arm
98 - V1 = 1.5*d*bw; % first guess of shear resistance
99 - V0 = 0; count = 0; % initiation of iteration
100 -
101 - while abs(V0-V1) > 10
102 - M0 = V1*d*mvd; % cross sectional moment
103 - w = M0/z/As/Es*lcrm; % estimation of average crack width eq..(4.8)
104 - V0 = V1;

```

Figure 3.8: Modified delta in MATLAB code

The modified shear force values are then documented for all the 8 slab specimens used in the experiment. The results are tabulated in Table 3.9

Table 3.9: Comparison of outputs for lower and upper bound limits using CSDT method excluding and including the slab factor respectively (Slab 8)

Symbol	Unit	Excluding Slab factor		Including Slab factor	
		Lower bound (substrate properties)	Upper bound (overlay properties)	Lower bound (substrate properties)	Upper bound (overlay properties)
OUTPUT					
Δ	mm	0.0103	0.0103	0.0113	0.0113
s_{cr}	mm	116.95	124.64	116.95	124.64
h_{cr}	mm	147.70	159.53	149.69	159.53
V_{ai}	kN	154.32	167.64	170.28	185.20
V_c	kN	127.37	122.98	134.99	130.13
V_d	kN	112.19	134.30	112.19	134.30
V	kN	393.88	424.92	417.47	449.62

Table 3.9 shows that with a slight increase in the delta values there is a consequential difference in the shear force values. This is especially for the shear force transmitted due to aggregate interlock and the uncracked concrete in compression zone mechanisms. The shear force transmitted due to dowel action is unaffected, as the delta value doesn't affect the dowel action mechanism which is also clear from the expression described in Equation 2.18.

After obtaining the lower and upper bound values for both the cases, an average value of the limiting cases is considered for direct comparison.

Table 3.10: Comparison of CSDT model with experimental results (Slab 8) after incorporating the slab factor (SF) (actual calculation)

Slab no.	Shear Force (experimental) (V_{exp}) [kN]	Average shear force excluding SF_{act} (V_{ESF}) [kN]	Average shear force including SF_{act} (V_{ISFact}) [kN]	V_{ESF}/V_{exp}	V_{ISFact}/V_{exp}
1	451.20	394.60	418.17	0.87	0.93
2	475.65	412.44	436.90	0.87	0.92
3	457.05	393.70	417.22	0.86	0.91
4	471.30	390.61	413.95	0.83	0.88
5	475.95	412.15	436.44	0.87	0.92
6	448.35	401.39	425.04	0.90	0.95
7	507.45	418.26	442.96	0.82	0.87
8	473.60	409.40	433.55	0.86	0.92
Mean Value				0.86	0.91

Table 3.10 shows the variation between the shear force values obtained directly from code and the shear force values obtained after incorporating the actual slab factor. The values inclusive of slab factor agree to the results of the experiment with a COV of 2.53 % as can be seen in Figure 5.1. Detailed calculations of actual slab factors for remaining slab specimens are given in appendix B in Figure B.6.

METHOD 2: SLAB FACTOR ESTIMATION (SF_{est})

In this method, the value estimated for slab factor is considered for further comparison. A factor of 1.182 (18.2 % increase) is recommended for RC slabs according to section 2.3.6. A sample calculation is done for slab specimen no. 8.

$$\begin{aligned}
 \text{Lower bound Shear Force } (V_{i,LB}) &= 393.88 \text{ kN} \\
 \text{Upper bound Shear Force } (V_{i,UB}) &= 424.92 \text{ kN} \\
 \text{Average of LB - UB } (V_{ESF}) &= 409.40 \text{ kN} \\
 \text{Enhanced Shear Force } (V_{ISFest}) &= 409.40 \times 1.182 = 483.91 \text{ kN} \quad (3.7) \\
 \text{Variation}_{old} (V_{ESF}/V_{exp}) &= \frac{409.40}{473.60} = 0.86 \\
 \text{Variation}_{new} (V_{ISFest}/V_{exp}) &= \frac{483.91}{473.60} = 1.02
 \end{aligned}$$

As shown in Table 3.7, for remaining slab specimens the same procedure is followed to obtain the shear force values. The results are as shown in Table 3.11.

Table 3.11: Comparison of CSDT model with experimental results (Slab 8) after incorporating the slab factor (SF) (approximation)

Slab no.	Shear Force (experimental) (V_{exp}) [kN]	Average shear force excluding SF_{est} (V_{ESF}) [kN]	Average shear force including SF_{est} (V_{ISFest}) [kN]	V_{ESF}/V_{exp}	V_{ISFest}/V_{exp}
1	451.20	394.60	466.42	0.87	1.03
2	475.65	412.44	487.50	0.87	1.02
3	457.05	393.70	465.35	0.86	1.02
4	471.30	390.61	461.70	0.83	0.98
5	475.95	412.15	487.16	0.87	1.02
6	448.35	401.39	474.44	0.90	1.06
7	507.45	418.26	494.38	0.82	0.97
8	473.60	409.40	483.91	0.86	1.02
Mean Value				0.86	1.02

As seen from Table 3.11, after incorporating the slab factor using approximation, the results obtained are most accurate with COV of 2.54 %. Though this method may produce results that resemble the experimental shear force values, its still an approximation unlike the slab factor calculated using actual parameters. Slab factor calculated using actual parameters is closest to reality. Thus, it is advisable to use SF_{act} for further calculation. Detailed calculations of slab factors are given in appendix B in Figure B.7 and B.8.

CRACK HEIGHT CHECK USING CSDT

As described in section 3.3.1, two cases are considered to be the limiting cases for a composite concrete slab, a homogeneous normal strength concrete slab and a homogeneous high strength concrete slab. Cracking pattern is observed for both these cases. The calculations are performed based on the critical shear displacement theory.

Sample calculation is carried out for slab no. 8 and the results are tabulated in Table 3.7 under the output head. The crack pattern will be discussed in this section. Detailed calculations of all slab specimens are given in appendix B Figure B.1.

As observed, the maximum vertical crack height obtained in both slabs is below 240 mm from bottom. This means that in all cases, the vertical crack is present only in the substrate region without it getting propagated further to the interface. This leads to the main equation described as per CSDT, i.e, Equation 3.3.4.

$$V = V_{ai} + V_c + V_d$$

As described in the research done by Dr. A. G. Mphonde [10], the contribution of aggregate interlock to concrete beams made of high strength concrete decreases significantly as the concrete compressive strength increases. Conversely, the contribution due to dowel action increases while that of the concrete in uncracked/compressive zone remains fairly constant as the concrete compressive strength increases.

- Contribution due to dowel action V'_d in above equation is obtained according to the plastic dowel mechanism and it has its influence only in the substrate region (normal strength concrete region). Hence, in this case, addition of an overlay irrespective of its material properties has no effect on the shear force transmitted due to dowel action.
- On the other hand, the contribution due to uncracked concrete V'_c is obtained considering equilibrium of forces in the composite slab cross-section and considering the high strength concrete overlay. Its effect on the shear force transmitted due to uncracked concrete is almost unaltered as material properties don't influence the equilibrium conditions.
- Thus, only the shear force transfer due to aggregate interlock action V'_{ai} is important in modifying the equation for a more general case for composite concrete members. It is, therefore, recommended to alter the limits of the integration in Equation 2.12 and Equation 2.14. As explained earlier, the contribution of aggregate interlock is reduced significantly in high strength concrete region. Thus, the maximum effect would be expected to happen in aggregate interlock in the substrate region while the effect in the HSC region will be handled by the uncracked concrete contribution as per the equilibrium conditions.

Crack distribution is later monitored in case of numerical analysis in order to check the variation of vertical crack height in case of composite concrete specimen. If the crack distribution is similar to the case as in the homogeneous slabs then the above recommendations can be applied for a composite concrete slab as well.

In the next section, stress distribution along the cross-section of a composite concrete slab is studied in order to support the argument that shear capacity of composite concrete slab can be calculated by assuming it to be homogeneous slab with substrate concrete material properties, with the dimensions as described in this report. Moreover, a check for a probable interface failure when the composite section is loaded in bending is performed. Again two different limiting cases are considered for the analysis. In the first case, there is no bond between the two concrete layers whereas, in the second case the two layers are perfectly bonded with each other. In both cases shear stress values at the interface are calculated depending on the governing scenarios. For uncoupled members (no bond), the governing case would be when the shear stress at interface is zero as there is no connection before cracks occur if any. While, in case of coupled members (perfect bond), the governing case is when cracks occur along the critical cross-section and there is redistribution of stresses. The slab will have minimum shear stress value in this case beyond which the bond will fail due to shear failure.

3.4. STRESS DISTRIBUTION ALONG A CRITICAL CROSS-SECTION OF COMPOSITE CONCRETE SLAB

In case of RC slab with a high strength concrete overlay applied on the deck, the interface between the two layers has to be tested for a possible failure mechanism. For this purpose, a shear check is performed to understand the slip behaviour of the interface between concrete (NSC)-concrete (HSC) bond.

3.4.1. CONCRETE-CONCRETE INTERFACE SHEAR CHECK

To perform the shear check, limiting values depicting the best and the worst case scenarios are considered. The worst case is when there is no bond between the concrete-concrete interface, i.e, the case of full slip behaviour. Whereas, the other case is when the concrete surfaces are fully bonded and exhibit a no-slip behaviour. In both the scenarios, critical cases will be considered to set the limiting shear stress values along a critical cross-section.

CASE 1: FULL SLIP/UNCOUPLED MEMBERS

In this case both the elements; concrete substrate slab and the HSC overlay are considered as two separate concrete members having no bond in the interface. This is the worst case possible for the model, as the full bearing capacity of the slab would not be used. The moment and the reaction forces on these members will be distributed according to the bending stiffness of the respective members.

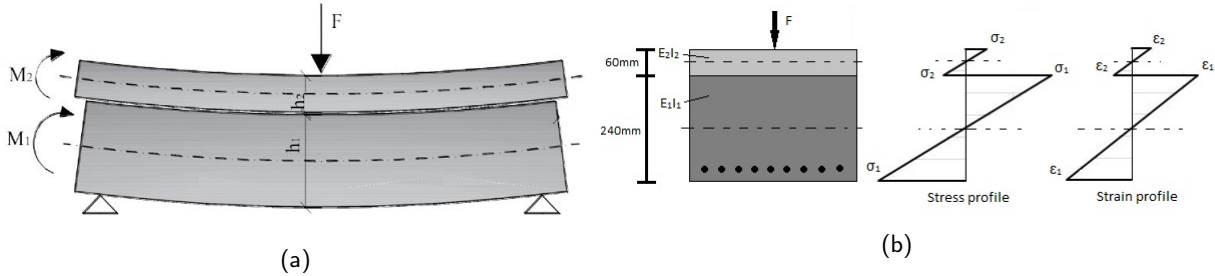


Figure 3.9: Uncoupled members (a) Loading (b) Stress and strain distribution along cross-section

$$\frac{1}{r_1} = \frac{1}{r_2}, \quad \frac{M_1}{E_1 I_1} = \frac{M_2}{E_2 I_2}, \quad M = M_1 + M_2, \tag{3.8}$$

$$\sigma_1 = \frac{M}{I_1 + I_2} \cdot \frac{h_1}{2}, \quad \sigma_2 = \frac{M}{I_1 + I_2} \cdot \frac{h_2}{2}$$

The curvature for both the members will be same in case there is no bond present in the interface. The Equation 3.8 explains the distribution of moment and stress in uncoupled members. As mentioned above, the normal stress data is used to calculate the shear stress along the cross section in both the concrete layers. In uncoupled members, the shear stress is zero at the end fibres of both concrete members and also at the interface. While, the fibres at the centroidal axis of bottom concrete slab has the maximum shear stress. The shear force distribution is same as that of the moment distribution in these members depending on their respective bending stiffness. Thus, considering the relations in Equation 3.8, the shear force distribution will be as shown in Equation 3.9.

$$\frac{V_1}{E_1 I_1} = \frac{V_2}{E_2 I_2} \tag{3.9}$$

Hence, the shear stress distribution can be approximated to be parabolic along the cross section of both the concrete layers, substrate as well as the overlay as can be seen in Figure 3.10. Detailed calculation of normal and shear stress is given in appendix B in Figures B.11 and B.13.

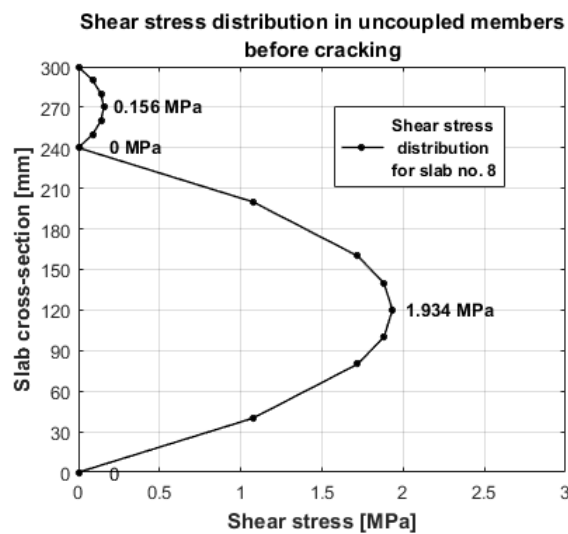


Figure 3.10: Shear stress distribution in uncoupled members

CASE 2: NO SLIP/COUPLED MEMBERS

Unlike the previous case, now the interface between the two concrete layers is fully bonded or there is no slip in the interface. Assuming a linear stress-strain relationship, following behaviour can be observed in the coupled members.

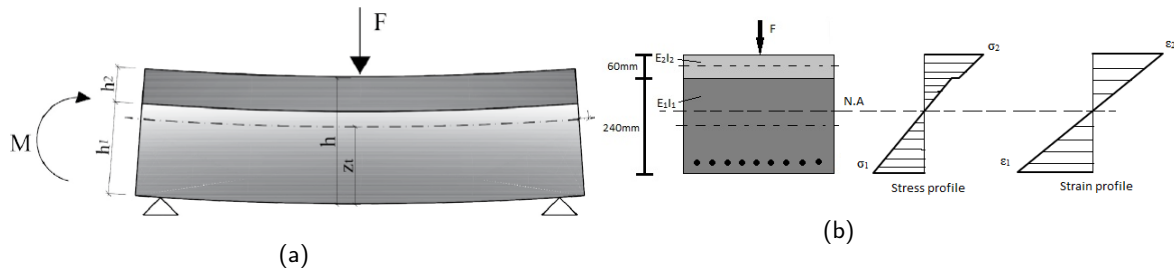


Figure 3.11: Coupled members (a) Loading (b) Stress and strain distribution along cross-section

The critical value of shear stress is obtained when the concrete member cracks and there is redistribution of stresses along the cross-section. N.D. Tung and N.V. Tue [5] in their research have proposed an approach for the shear design of slender concrete members without transverse reinforcement taking into consideration the stress redistribution once the member cracks. For this, they took into account the normal stress in concrete tension zone, which is often neglected. They further explain that damage is normally localized in a narrow band in the concrete tension zone just below the compressive zone which eventually results in the creation of a critical inclined crack. Detailed stress distribution calculation along the cross-section, in case of coupled members, is given in appendix B in Figure B.12 and Figures B.14 - B.17.

To calculate the stress distribution along the cross-section, the concept of equivalent area is used, as the stiffness difference needs to be accounted for. For this, the width of the overlay concrete member is multiplied by a factor 'r'. A new composite cross-section is developed considering a uniform elasticity modulus of the substrate concrete member for the entire section;

r is the ratio between the elastic modulus of overlay to that of the substrate concrete layer, $r = E_o/E_s$.

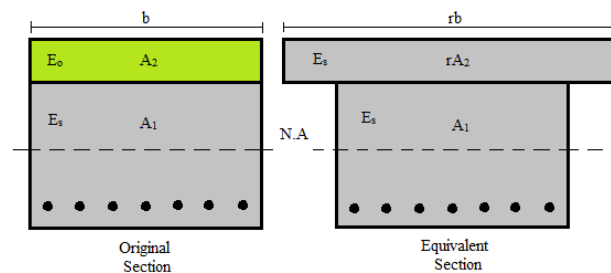


Figure 3.12: Equivalent area method

The concept of shear band is introduced in the report by Tung and Tue [5]. In their research, they explain that the formation of a critical shear crack takes place through coalescence of the micro cracks in a shear band in the concrete tensile zone. When this shear band reaches a critical width, the critical inclined crack is formed. This critical shear band width depends on the concrete fracture properties and the concrete strains in the tension zone.

- Concrete strength: The crack propagation behaviour is aided by a high strength concrete member since it is brittle in nature. Thus, the critical width of shear band is decreased with the increase of concrete strength
- Reinforcement ratio: The crack propagation is favoured with a larger reinforcement ratio, thus, with the increase in the reinforcement ratio, the critical width of the shear band also increases.

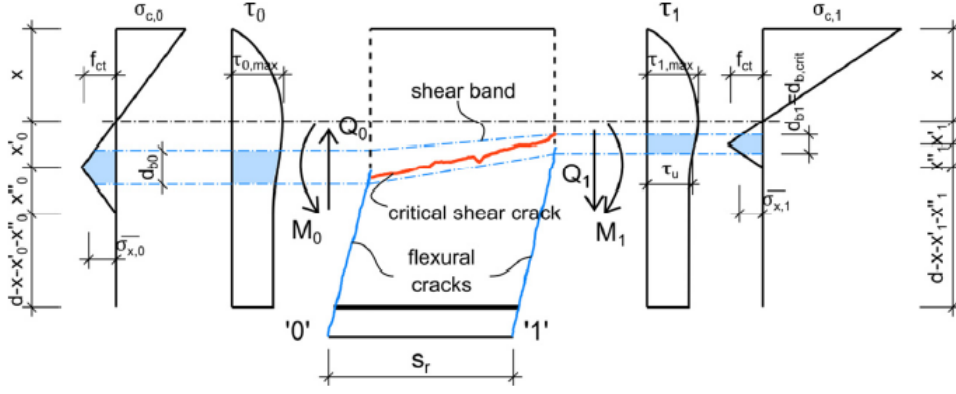


Figure 3.13: Normal and shear stress of concrete in a segment between two primary flexural cracks [5]

In the above Figure 3.13, the stress distribution according to Tung and Tue can be seen. A main assumption considered in this theory is that, even the cracks appear diagonal for calculation purposes and simplification of the model, a vertical crack is considered to estimate the normal and shear stresses at the cross-sections. The steps involved in calculating the shear stress along the cracked cross-section in a concrete member are given by Equations 3.10 - 3.19.

$$d_{b,crit} = 0.5 \cdot \frac{(100\rho_s)^{0.9}}{f_c} \quad (3.10)$$

$$x' = \frac{\varepsilon_{ct}}{\varepsilon_c} \cdot (d - x) \quad (3.11)$$

$$\varepsilon_s = \frac{1}{E_s \cdot \rho_s \cdot b_w \cdot d} \cdot \left(\frac{M}{z} + \frac{V}{2} \right) \leq \frac{1}{E_s \cdot \rho_s \cdot b_w \cdot d} \cdot \left(\frac{M_{max}}{z} \right) \quad (3.12)$$

$$x = \left[\sqrt{(\rho_s \cdot n)^2 + 2\rho_s \cdot n - \rho_s} \cdot n \right] \cdot d \quad (3.13)$$

$$\begin{aligned} f_{ct} &= 0.3(f_{ck})^{2/3} && \text{for concrete grades } \leq C50 \\ &= 2.12 \ln(1 + 0.1f_c) && \text{for concrete grades } > C50 \end{aligned} \quad (3.14)$$

$$x'' = \frac{G_f}{f_{ct} \cdot w_k} \cdot (d - x - x') \quad (3.15)$$

$$\begin{aligned} w_k &= s_{rm} \cdot (\varepsilon_{sm} - \varepsilon_{cm}) \\ &= s_{rm} \cdot \frac{1}{E_s} \cdot \left[\sigma_s - 0.5 \cdot \frac{f_{ct}}{\rho_{p,eff}} \left(1 + n \cdot \rho_{p,eff} \right) \right] \end{aligned} \quad (3.16)$$

$$\begin{aligned} \sigma_{xm} &= f_{ct} \cdot \left(1 - 0.5 \cdot \frac{d_{b,crit}}{x' + x''} \right) && \text{if } d_{b,crit} < x' + x'' \\ &= f_{ct} \cdot \left(0.5 \cdot \frac{d_{b,crit}}{x' + x''} \right) && \text{if } d_{b,crit} \geq x' + x'' \end{aligned} \quad (3.17)$$

$$\tau_u = \sqrt{f_{ct} \cdot (f_{ct} - \sigma_{xm})} \quad (3.18)$$

$$\tau_{max} = \frac{\tau_u}{1 - \left(\frac{x'}{d} \right)^2} \quad (3.19)$$

$$\tau_{Rc} = \frac{2/3\tau_{max} \cdot x + 1/2(\tau_{max} + \tau_u) \cdot x' + \tau_u \cdot (d - x - x')}{d}$$

where,

- b_w : width of the member
- d : effective depth of member
- $d_{b,crit}$: critical width of the shear band
- f_c : compressive strength of concrete
- f_{ct} : tensile strength of concrete
- G_f : fracture energy of concrete
- n : modular ratio for reinforcement steel
- s_{rm} : crack spacing of primary cracks
- w_k : primary cracks crack width
- x : neutral axis depth of cracked concrete section
- x' : distance from the peak of the concrete tensile stress to the N.A
- x'' : height of the region with softening of concrete in the tension zone
- ϵ_{ct} : strain of concrete by reaching tensile strength
- ϵ_s : strain in longitudinal rebar
- ρ_s : reinforcement ratio
- $\rho_{p,eff}$: reinforcement ratio in the effective area near the rebars
- τ_u : allowable shear stress in the critical width of the shear band
- τ_{max} : maximum shear stress at neutral axis
- τ_{Rc} : relative shear capacity, $\tau_{Rc} = V_{Rc}/(bd)$
- σ_{xm} : average normal stress of concrete in the shear band width

From the above relations, the shear stress along a coupled member cross-section is calculated using the equivalent area method as shown in Figure 3.12. The shear stress distribution is as shown below. Figure 3.14 shows the shear stress distribution of specimen no. 8.

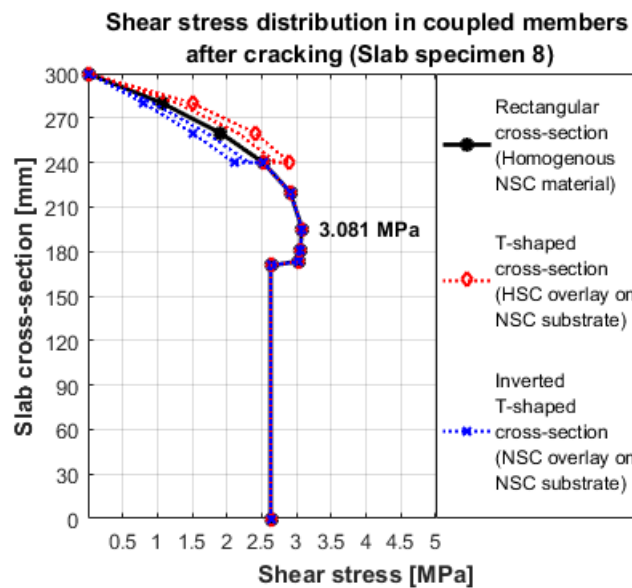


Figure 3.14: Shear stress distribution in coupled members after cracking (for slab no. 8)

The variation of shear stress at the interface as shown in Figure 3.14 is because the value at the interface cannot be found out perfectly with the help of the analytical models. But, the maximum value of shear stress in the substrate region can be calculated perfectly. Thus, it is assumed that the value at interface won't exceed the maximum allowable shear stress value, since, the overlay is still in elastic region as cracks haven't reached the interface level. In the Figure 3.14, the red curve denotes the estimated shear stress distribution in case when a high strength concrete overlay is applied over the NSC substrate. Whereas, the blue curve represents the estimated shear stress distribution in case a normal strength concrete overlay is applied over the NSC substrate.

Another important assumption in the analytical model proposed by Tung and Tue [5] is that the crack which initiates at the critical moment is vertical in nature. This gives a stress distribution as shown in Figure 3.13. For further verification of the numerical model, shear stress at a cracked section where the initial crack is vertical in nature is compared with the analytical model in further sections.

In the next chapter the stress distribution along the cross-section of a composite concrete slab in a numerical model is analyzed and a correlation between the analytical and numerical results is shown. The shear stress between the composite slab specimen, NSC homogeneous slab and HSC homogeneous slab is also compared to further support the argument that the shear capacity of a composite slab specimen, such as described in this report, can be calculated by assuming it to be a NSC concrete homogeneous slab with same dimensions. Moreover, the shear stress distribution along the interface is checked for a possible de-bonding in the numerical model to verify the interface behaviour with the experimental observations.

4

Numerical Model using ATENA

According to the new fib Model Code 2010, the design shear resistance of a reinforced concrete (RC) structure can be evaluated through analytical and numerical calculation methods that fall into four different levels of approximations. The complexity and the accuracy of the calculated shear resistance increase with increasing the level of approximation. Nonlinear finite element analysis (NLFEA) belongs to the highest level of approximation (Level IV) because of their advantage to consider real material properties and some more 'hidden' capacities of the structure [11]. In today's world NLFEA is used as a basic step to simulate real-life situations. Since in olden times such advanced models were not developed, to check the service life and durability of existing structures, many companies especially in Netherlands, are using NLFEA. ATENA is used especially in case of concrete structures as it provides ease in developing a structural model with concrete material and gives accurate results while studying the stress-strain properties, creep, shrinkage and strength properties. Figure 4.1 shows the experimental set-up of the four-point bending test performed on a RC slab with a HSC overlay as also described before in section 3.2.

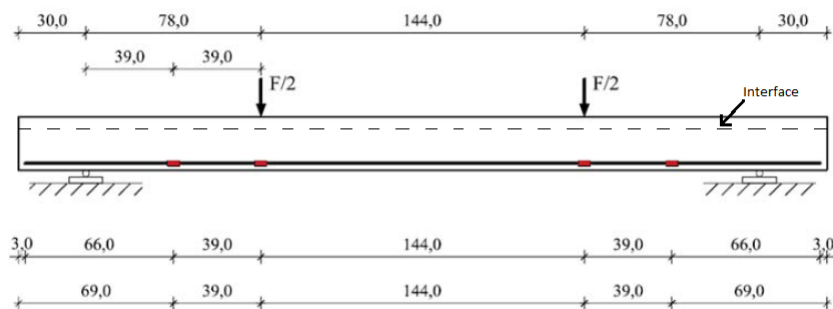


Figure 4.1: Test setup for 4-point bending test [4] [all dimensions are in cm]

4.1. NUMERICAL MODEL

4.1.1. INTRODUCTION ON FE MODEL CREATION

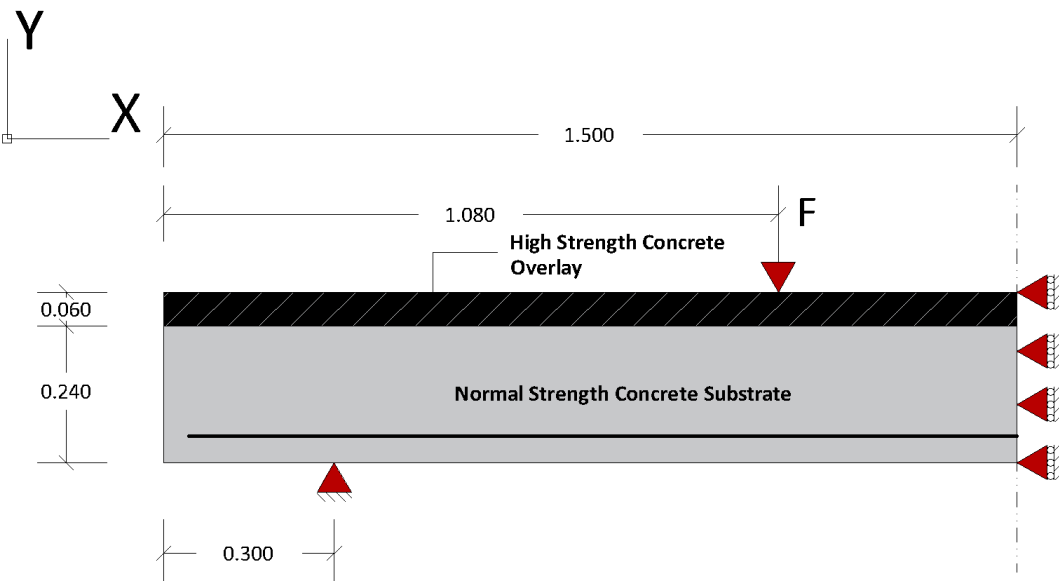


Figure 4.2: Details of test specimen using symmetry (All measurements are in meters)

Figure 4.2 shows the test specimen depicting the actual experimental loading and boundary conditions. It is a four-point bending test. However, only half of the slab is modelled using symmetry along a vertical axis through the mid-plane of the slab. For ease of modeling the reinforcement details shown in bottom only consists of the longitudinal main reinforcement as shown in the reinforcement configuration of Figure 3.1. This is also done because in bending, the main reinforcement is more important than the transverse reinforcement, which is placed mainly to hold the main rebar together.

The bottom part of the slab is a normal strength concrete while the shaded region above it, is a high strength concrete overlay in Figure 4.2. ' F ' is a point force acting on one half of the slab such that total force acting on the slab is ' $2F$ '. The bottom left support restricts the translation in y -direction while the roller supports on the right most edge of the slab, restricts the movement in only x -direction and allows translation in vertical direction. Actual test set-up is shown in Figure 3.5.

4.1.2. COMMENTS ON FE MODEL PREPARATION

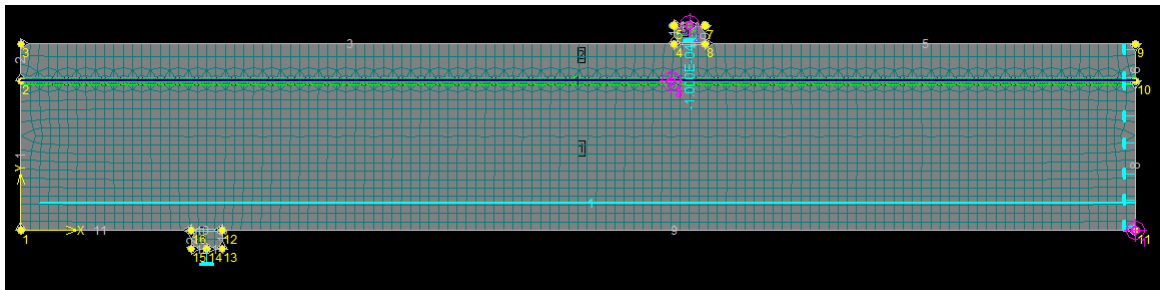


Figure 4.3: Finite element model used for analyzing cracking pattern in RC slab with HSC overlay on top

Figure 4.3 shows the FE model created for slab specimen no. 8. The material properties and other input parameters are prescribed as follows.

MATERIALS

Concrete of both slabs (overlay and substrate) is modeled by 'Non-linear cementitious' material model, with parameters given in Table 4.1. Material of the reinforcement is represented by Bilinear Von Mises stress model (Table 4.2). In addition, the concrete-concrete 2D interface and the 2D interface between steel plate and concrete both are modeled with properties as described in Table 4.3. Also, the steel plate model properties are given in Table 4.4 which are designed using the plane stress elastic isotropic model.

TOPOLOGY

Design of the model is distributed among four macroelements representing the two concrete slabs; substrate and overlay, and the two steel plates used for load application and support conditions. The connection between the two concrete surfaces is specified as 2D interface, gap type with a mesh refinement as per number of elements. Similarly, the connection between steel plates and their respective concrete slab is also specified as 2D interface, gap type but mesh refinement is not applied for these interfaces. The previously defined interface models are assigned to these interfaces.

LOADS AND SUPPORTS AND RUN

As symmetry is used to design the model, support to the left is fixed in y-direction and is applied as a point support. Whereas, the right edge of the half-slab model is fixed in x-direction and is applied as line support (load case LC1). A point load is applied at mid point of the top steel plate by prescribing uniform vertical displacement of 0.1 mm (load case LC2). The loading is applied with a step multiplier of 2 in 140 load steps. The Modified Newton-Raphson solution method with parameters listed in Table 4.5 is employed. The finite element mesh properties are defined in Table 4.6. Thickness of the macroelements is defined as 1.0 m as per the dimensions of the RC slab defined in Figure 3.1. The overall response is recorded at two monitoring points - loading as reaction at the top loading point and displacement at the bottom of the slab on the symmetry plane.

Table 4.1: Material properties of concrete

Material type	Symbol	Non Linear cementitious material	Units
Overlay			
Elastic Modulus	E_o	37450	MPa
Poisson's ratio	ν	0.2	-
Compressive cube strength	$f_{c,cube}$	98.79	MPa
Tensile strength	f_t	5.75	MPa
Crack Model		Fixed	
Substrate			
Elastic Modulus	E_s	28990	MPa
Poisson's ratio	ν	0.2	-
Compressive cube strength	$f_{c,cube}$	57.28	MPa
Tensile strength	f_t	4.82	MPa
Crack Model		Fixed	

Table 4.2: Material properties of reinforcement

Material type	Symbol	Bilinear steel Von Mises	Units
Elastic Modulus	E_{steel}	210	GPa
Yield strength	σ_y	550	MPa

Table 4.3: Material properties of interfaces

Material type	Symbol	2D Interface	Units
Concrete-concrete interface			
Normal stiffness	K_{nn}	1.4×10^8	MN/m^3
Tangential stiffness	K_{tt}	1.4×10^8	MN/m^3
Tensile strength	f_t	4.80	MPa
Cohesion	c	1.70	MPa
Friction coefficient	μ	0.6	-
Steel (Steel plate)-concrete interface			
Normal stiffness	K_{nn}	2×10^{10}	MN/m^3
Tangential stiffness	K_{tt}	2×10^{10}	MN/m^3
Tensile strength	f_t	0	MPa
Cohesion	c	0	MPa
Friction coefficient	μ	0.5	-

Table 4.4: Material properties of steel plates

Material type	Symbol	Plane stress elastic isotropic	Units
Elastic Modulus	E_{steel}	210	GPa
Poisson's ratio	ν	0.3	-

Table 4.5: Solution parameters

Solution method	Newton-Raphson (Modified)	
Stiffness/update	Elastic/each step	
Number of iterations	40	
Error tolerance	0.01	
Line search	on, with iterations	

Table 4.6: Finite element mesh

Finite element type	concrete	Quadrilateral (CCIsoQuad)	
Finite element type	steel plates	Quadrilateral (CCIsoQuad)	
FE mesh element size	concrete	15	mm
FE mesh element size	steel plates	20	mm
Element shape smoothing		on	
Optimization		Sloan	

Results and Discussion

Simulations run using ATENA software have been compared with the experimental as well as analytical results. Discussions explaining the nature of the results are also documented in this chapter. The results obtained are very helpful in understanding the behaviour of the finite element model.

5.1. RESULTS

Table 5.1: Comparison of three shear models with experimental results

Slab no.	(V_{EC}/V_{exp})	(V_{CSCT}/V_{exp})	(V_{ISFact}/V_{exp}) (with SF_{act})	(V_{ISFest}/V_{exp}) (with SF_{est})
1	0.54	1.07	0.93	1.03
2	0.57	1.13	0.92	1.02
3	0.53	1.05	0.91	1.02
4	0.51	1.00	0.88	0.98
5	0.58	1.15	0.92	1.02
6	0.60	1.20	0.95	1.06
7	0.55	1.08	0.87	0.97
8	0.58	1.15	0.92	1.02
Mean Value	0.56	1.10	0.91	1.02
COV	4.99 %	5.54 %	2.53 %	2.54 %

A summary of the three shear models compared in the previous sections is tabulated in Table 5.1. In Figure 5.1, all the coefficients of variations are compared as per the aforementioned methods. Detailed calculation of the coefficients of variation is given in B in Figure B.9. The red data points represent the shear stress in HSC homogeneous concrete slab (upper bound). Whereas, the blue data points represent shear stress in NSC homogeneous concrete slab (lower bound) and the black data points represent average of these two values. The comparison among the COV clearly shows the accuracy of CSCT method. Here, the ratio between the shear force values due to analytical model and experimental results is closest to unity (or the diagonal line shown in the graphs). The cluster of data is densely located in these two graphs as the COV is closest to zero, especially when the slab factor (SF_{act}) is incorporated with actual calculated method.

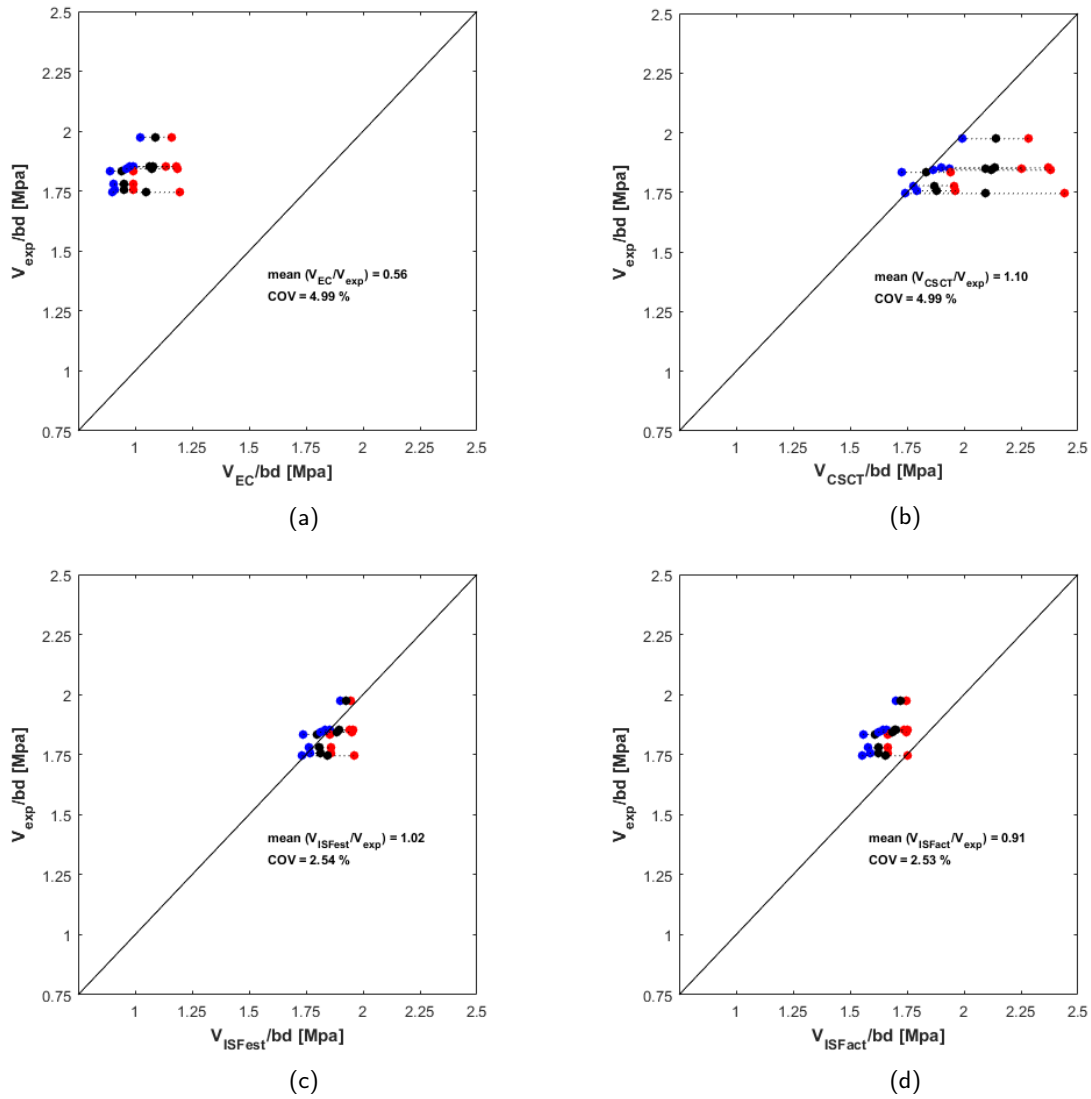


Figure 5.1: Comparison of shear models (a) Eurocode 2; (b) CSCT; (c) CSDT (Slab factor estimation) (d) CSDT (Slab factor actual calculation)

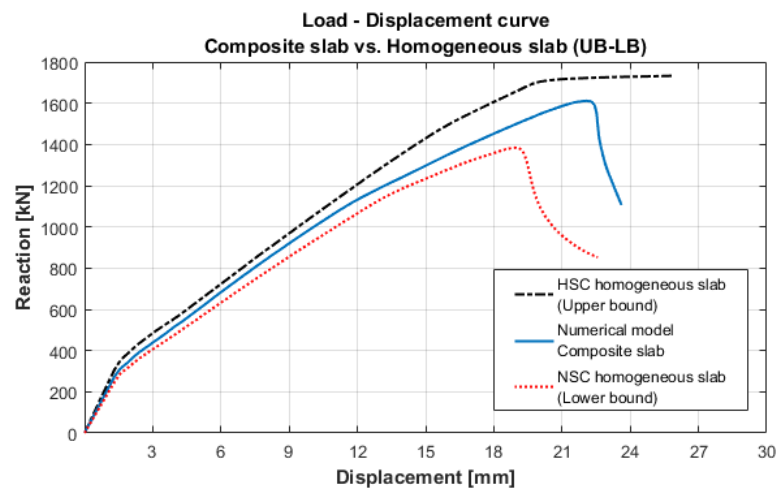


Figure 5.2: Comparison of numerical results between Composite slab (Slab no.8) and homogeneous slab

Figure 5.2 shows a comparison between the numerical results obtained from slab specimen 8, that is the composite slab and the two homogeneous models that are made of high strength concrete and normal strength concrete, depicting the upper and the lower bound limits, respectively.

The load displacement curve for the composite slab specimen lies in between the two graphs which justify the assumption made in section 3.3.1. Moreover, the load - displacement curve for the composite slab specimen and the curve with normal strength concrete properties are very similar in nature. Both the graphs show a brittle behaviour as compared to the high strength concrete homogeneous slab which shows a ductile behaviour. Although, the load carrying capacity of the composite slab lies in between the two limiting cases, failure behaviour in the former two cases is rather comparable.

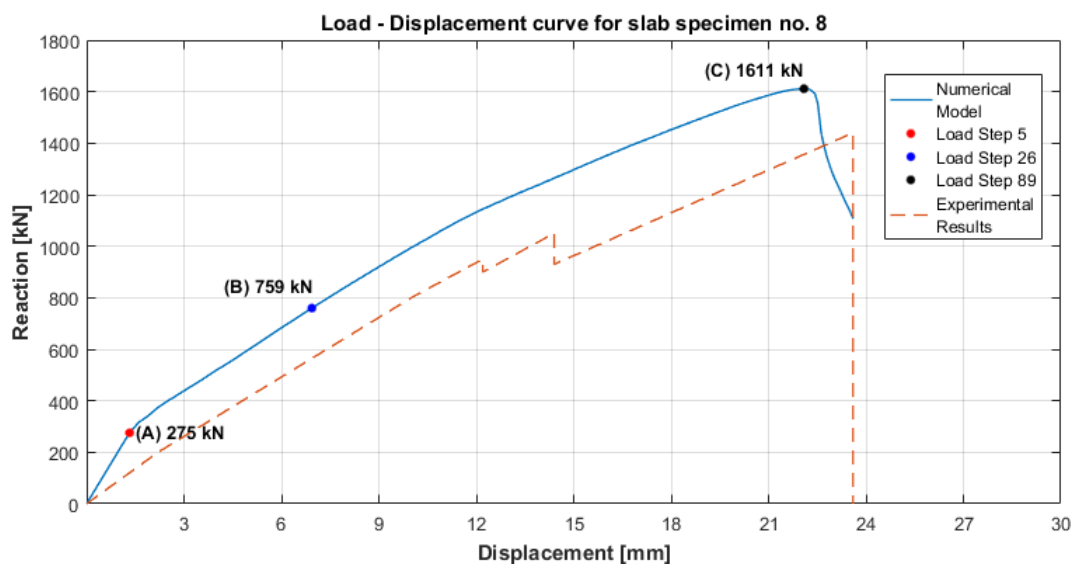
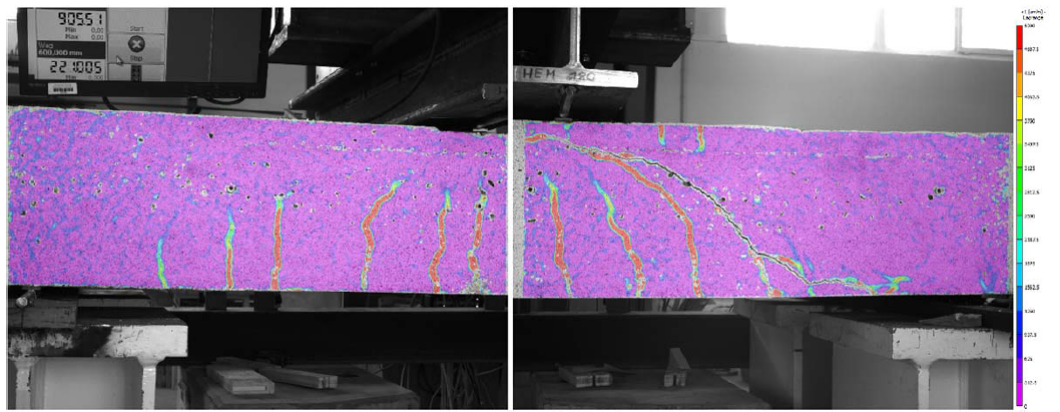


Figure 5.3: Comparison between experimental (platte 8_Rt=0.8mm) [4] and numerical model (Slab no.8)

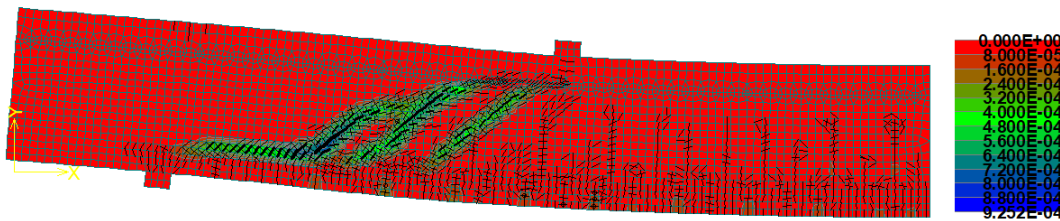
In Figure 5.3, a comparison between experimental results for slab plate no. 8 ($R_t = 0.8\text{mm}$) and numerical results obtained by NLFEA of slab specimen no. 8 is shown. The nature of graph obtained by the numerical model is similar to that of the experiment, which means the numerical model agrees with a real time experimental slab model. Although, a slight difference can be observed in the initial stiffness between the two graphs. This can be due to a certain level of in-homogeneity in the real time concrete member composition which is completely ignored while modeling the slab in ATENA. This reason also explains the slight difference between the peak load values in experiment and in numerical model. Three representative load steps are marked in the numerical model graph namely; A, B and C.

- Point A represents load step no. 5 (displacement of the bottom most node on the symmetry axis reaches 1.33 mm) at which the concrete slab bottom-most fibres reach their tensile strength and start to crack.
- Point B represents load step no. 26 (displacement of the bottom most node on the symmetry axis reaches 6.94mm) at which the initiation of the critical inclined crack takes place.
- Finally, point C represents load step no. 89 (displacement of the bottom most node on the symmetry axis reaches 22.10mm) which is the maximum load the concrete slab can carry, in other words the load carrying capacity of the composite concrete slab.

Crack profile obtained in the numerical analysis is now compared with the experimental cracking pattern observed by Dr. Randl.



(a) Crack pattern observed in experiment carried out in lab [4]

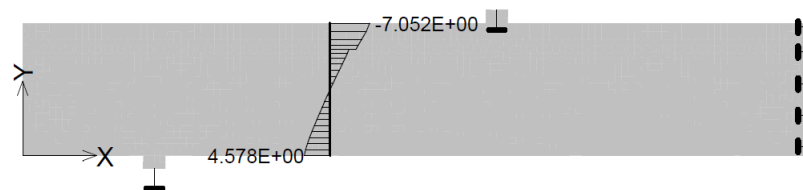


(b) Crack pattern obtained in numerical model of slab specimen no.8 modeled using symmetry (deformed shape of slab with scale = 5.0)

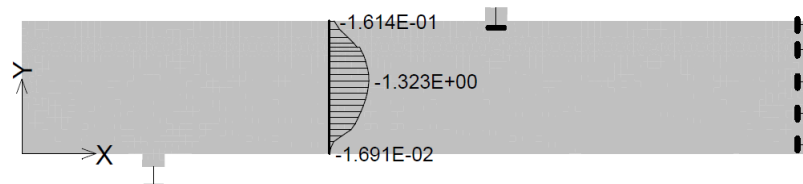
Figure 5.4: Comparison of cracking pattern between experimental and numerical model

The cracking pattern obtained, in case of monotonic loading, with the numerical model agrees with the experimental results which is diagonal in nature in both models, thus further validating the model. In the experiment, further load increment does not lead to failure of the interface between the two concrete layers. Similarly on further increasing the prescribed deformation in the numerical model, the crack slowly propagates through the interface and then in the high strength concrete overlay but does not lead to failure of the interface. The numerical failure mode was due to the diagonal critical crack formation, which caused collapse of the slab if the loading is further increased. Further research can be done in case of dynamic loading.

NORMAL AND SHEAR STRESS DISTRIBUTION IN CONCRETE SLAB BEFORE AND AFTER CRACKING



(a) Normal stress distribution before cracking in the shear span



(b) Shear stress distribution before cracking in the shear span

Figure 5.5: Normal and shear stress distribution in numerical model before and after cracking of the shear span

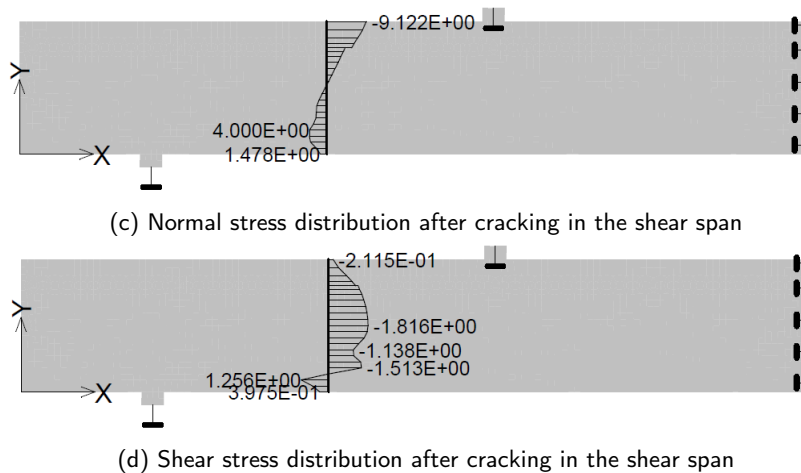


Figure 5.5: Normal and shear stress distribution in numerical model before and after cracking of the shear span (contd.)

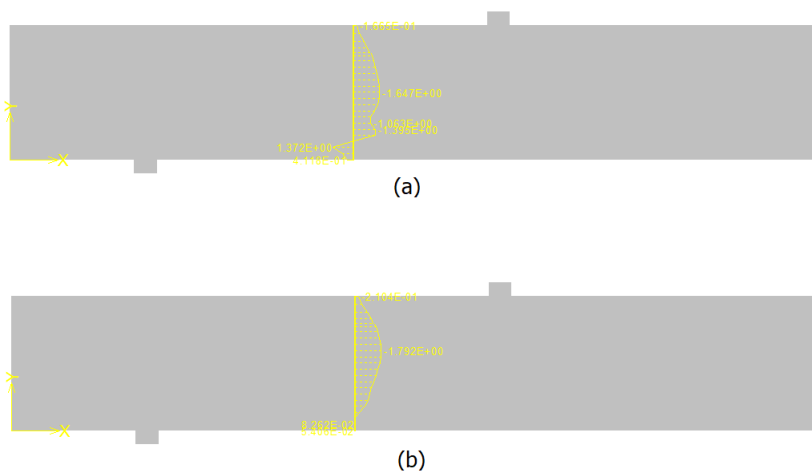


Figure 5.6: Shear stress distribution in (a) NSC homogeneous slab and (b) HSC homogeneous slab

In this section a validation to the argument that a composite concrete slab can be assumed to be a homogeneous slab with substrate concrete properties, with the dimensions as provided in this report, for estimating the shear capacity of a composite concrete slab.

From Figures 5.5a and 5.5b, the elastic behaviour of concrete before the slab starts cracking in the shear slab is evident from the linear stress distribution of normal stress and an approximate parabolic distribution of shear stress. On the other hand, Figures 5.5c and 5.5d explain the non-linear behaviour of concrete which corresponds to the stress distribution obtained by analytical methods in Figures 3.13 and 3.14. The critical cross-sections shown in the above figures are shown at such load steps where the cracks occurring at these respective cross-sections are vertical thus, satisfying the main assumption considered in the model proposed by Tung and Tue. However, a minor difference between the analytical and numerical stress results is observed in the bottom part of both the stress distributions after occurrence of vertical cracks. This is as a result of an approximation in the analytical model that no other cracks appear, not even micro cracks, near the vertical crack at the bottom fibre. While, in reality there are always cracks present in the vicinity of the vertical crack which gives a difference in the stress distributions near the bottom fibre.

In Figure 5.6, the shear stress distribution at critical cross-sections is shown for two homogeneous concrete slab cases. First case (a) is for normal strength concrete (NSC) homogeneous slab and second case (b) is for high strength concrete (HSC) homogeneous slab. Shear stress distribution in Figure 5.5d resembles with

the results in the NSC homogeneous slab shear stress distribution. Thus, this further proves the correlation between the normal strength concrete homogeneous slab and the composite concrete slab.

Figure 5.7 shows the shear stress distribution along the interface of the composite concrete specimen. The maximum value at the interface for shear stress is around 0.88 MPa and the shear diagonal failure has already occurred. This means there is no failure at the interface in such loading conditions. Shear failure of the substrate is governing for this analysis which is evident from the experimental results as well.

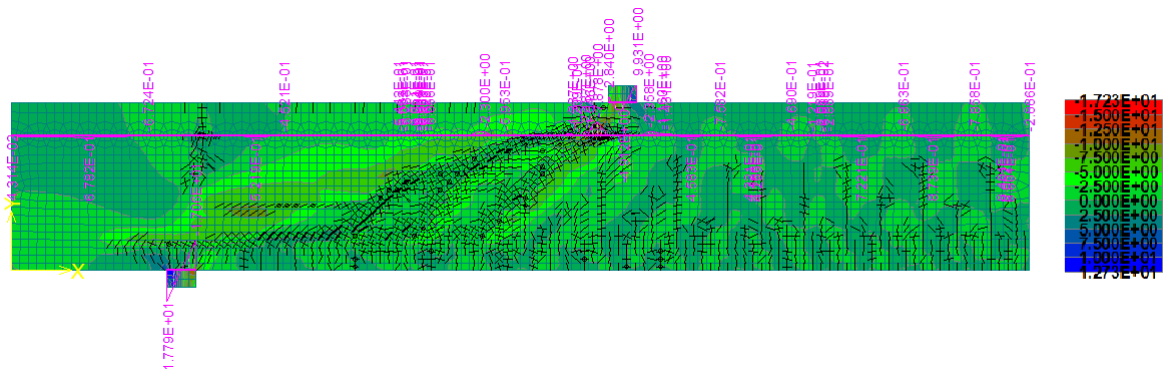


Figure 5.7: Shear stress distribution at the interface of the composite concrete slab

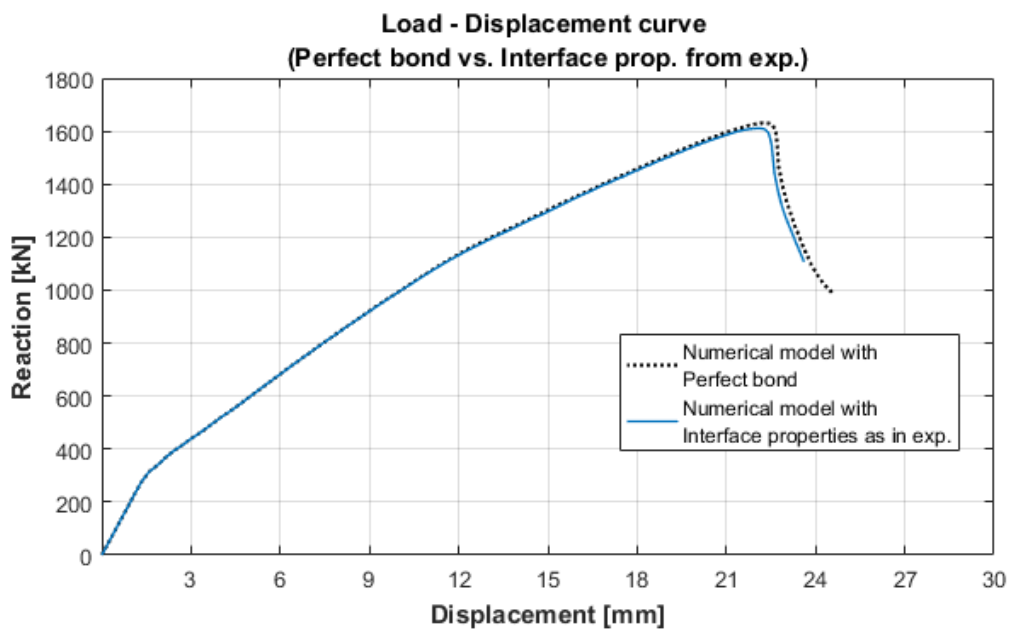


Figure 5.8: Comparison of numerical models with perfect bond and interface properties from experiment

Another comparison is carried out between a perfectly bonded composite slab and another one with interface properties as given in Table 4.3. As can be seen from Figure 5.8, the force displacement curve for the perfectly bonded specimen has a slightly higher load carrying capacity than the slab with the given interface properties. The difference between the two models is not significant because the interface properties assigned to the model has a tensile strength almost equal to the substrate concrete tensile strength, which makes the model resemble closely to a perfectly bonded specimen.

5.2. DISCUSSION

Guidelines for examining the behaviour of a composite concrete slab, under examination of a point load or uniformly distributed load are not available. But in case of a homogeneous concrete slab or beam, various theories and models are already defined. Therefore, as a first step the behaviour of a homogeneous concrete slab is studied. This develops some basis for guidelines to proceed with the study of a composite concrete slab element. Out of the various models available, three shear models are studied in this work; the Eurocode 2, the Critical shear crack theory (CSCT) and the Critical shear displacement theory (CSDT).

In section 3.3.1, for each slab specimen tested by *Dr. Randl*, two cases are considered. The first one as a homogeneous slab with exclusively the substrate concrete layer properties (normal strength concrete NSC) and second one as a homogeneous slab with only overlay concrete layer properties (high strength concrete HSC). As a result, two limiting values are obtained for each composite concrete slab specimen. Shear resistances obtained from three shear models are used as a measure of direct comparison between these models. These values are considered as the lower and upper bound limiting values for estimating the shear resistance of a composite slab. An average of these limiting values is calculated for each shear model which are then compared directly to each other and with the experimental shear resistances. Furthermore, the variation of these results is documented.

The results obtained by adopting the procedure specified in Eurocode2 fetches results having least accuracy giving a mean variation of 0.56 with COV 4.99 %. Whereas, by using critical shear crack theory the accuracy is improved substantially giving mean variation of 1.10 but a COV of 5.54 %, which is still not in allowable limits. The critical shear displacement theory gives the most accurate results with mean variation of 0.91-1.02 depending on the two different slab factor methods and COV of almost 2.53 % for both methods considered. The mean variation as close to unity and the COV as close to zero, is better for acceptability of the model. This is achieved when shear force is calculated using CSDT.

In the procedure prescribed by Eurocode2, number of assumptions are made to calculate the shear capacity of a concrete member. This is evident from the use of various factors in the formulae leading to the shear capacity of the concrete member. Also, the effect of concrete in compressive zone is neglected while calculating the shear capacity. In the critical shear crack theory, contribution of the concrete in compressive zone is taken into consideration to improve the accuracy of results. The micro cracks in the shear band 3.4.1, which subsequently lead to the critical inclined crack, improve the shear capacity of the concrete member. This can be explained by the strut and tie phenomenon. Finally, in the critical shear displacement theory, the effect of the vertical displacement caused by cracking is also taken into consideration along-with the effect of concrete in compressive zone. In case of a concrete slab, the vertical displacement caused by cracking of the secondary diagonal crack (Figure 2.3), leading from a vertical crack, increases the shear capacity substantially. Moreover, a cracking pattern is obtained in the transverse direction along all the weak spots that enhances the aggregate interlocking effect along the cracked planes. For example, in case of concrete beams the maximum vertical shear displacement is achieved as soon as the entire cross-section cracks along the width of the beam. Whereas, in case of concrete slab, width of the member is much larger as compared to a concrete beam, thus a greater force is required to induce cracks throughout the width of the slab. Moreover, the reinforcement quantity is substantially higher in slabs. A higher shear force is needed to achieve necessary crack width throughout the width in order to activate yielding of reinforcement. As the dowel action is a plastic phenomenon, reinforcement in the slab has to reach its plastic state for full effect on shear transfer by dowel action. This greater shear force is thus responsible for the maximum shear displacement. In other words, the critical shear displacement theory is an advanced version of critical shear crack theory.

The model described by CSDT is mainly developed for homogeneous concrete beams, wherein the width of the specimen is very small as compared to width of a slab. However, as described before, load bearing capacity of a slab is much higher than a concrete beam if rest two dimensions and material properties are kept constant. In a slab the cracking pattern is not uniform but it can rather be approximated as a wave pattern having its own amplitude and wave length, which determine the spread of the cracks and their behaviour in the longitudinal direction. This phenomenon of wavy crack pattern in addition to higher quantity of longitudinal reinforcement, leads to an increase in the vertical shear displacement of the slab which is a substantial increment. This enhanced vertical displacement gives a boost to the shear capacity by increasing the aggregate interlock resistance thereby increasing the load carrying capacity of the slab. A

slab factor is introduced confirming the effect of both amplitude and wave length of the cracking profile. It is calculated using two methods, first one, uses an exact calculation technique. In this method, wavelength and amplitude of the crack profile are calculated, depending on the material parameters. Thus, an effective width is calculated along-with the enhanced vertical shear displacement, which in turn increases the final load carrying capacity by increasing the resistance due to aggregate interlock. Another method to calculate the slab factor is by using an approximation as proposed by Yang. He proposes a rise in the final load carrying capacity by 18.2 %. The results obtained by the second method agree with the experimental results perfectly but after all it is an ideal approximation. The first method is based on realistic crack distribution and the exact calculation improves the accuracy of the method as well.

In high strength concrete material the contribution of aggregate interlock reduces significantly, as the cracks in the specimen go through the aggregate rather than around them (along the cement-aggregate boundary) which is usually the case in normal strength concrete specimen. Also, the contribution due to dowel action increases while that of uncracked concrete is approximately constant [10]. An important observation in the case of composite concrete slab specimens with an overlay on top of NSC slab referring to the CSDT is that, as, only the shear force transferred due to aggregate interlock V'_{ai} is mainly affected in the substrate region, thus, modifications to the aggregate interlock parameter in the formulae, proposed in CSDT, are prescribed. The limits for the shear resistance transferred through aggregate interlock can be changed to the substrate slab thickness dimension. The expression for shear force transferred due to dowel action will be unaltered as, new material is introduced on top of the slab which does not affect the reinforcement-concrete bond keeping the value V'_d constant. Whereas, uncracked concrete's contribution V'_c will be calculated as per the equilibrium in the system. Thus, shear capacity of a composite concrete slab can be estimated by considering the substrate concrete properties mainly for the calculation of shear resistances transferred due to aggregate interlock, longitudinal reinforcement dowel action, the uncracked concrete and some residual stresses in the secondary diagonal crack.

For further validation of the above argument, effect of bond between the two concrete layers is also studied. For this, two cases are considered; one with no bond and another with perfect bond between the concrete layers. Results are also compared with analytical methods, where stress distribution at a critical cross-section is compared. To obtain the values of stress at a cross-section using analytical methods, the composite slab is considered as one slab with homogeneous material and equivalent area method is used to determine these values. Hence, in the shear stress distribution graph in Figure 3.14, the black line represents a rectangular cross-section and the graph follows smoothly governing a parabolic equation. However, in case, if a HSC overlay is applied on top of NSC substrate, then by equivalent area method the width of top overlay will increase and the cross-section will appear to be T-shaped. Similarly, in case of a NSC overlay the cross-section will appear as inverted T-shaped. Hence, the red and blue lines representing the same behavior.

There is striking similarity in the stress distribution obtained in the numerical analysis and results from analytical propositions, except at the bottom fibres. This is because in the analytical model, although cracks in the slab appear to be inclined, for simplification of model and ease in calculation, it is assumed that there are only vertical cracks present at regular spacing. Whereas, in the numerical model the cracks are distributed throughout the bottom part of the slab with very few vertical cracks in the first half of the analysis. Eventually, some vertical cracks can be observed in the shear span of the slab before their development into a diagonal inclined crack. This can also be visualized as a strut-tie cracking model. Furthermore, a comparison between HSC and NSC homogeneous slabs and the composite concrete slab is carried out. The shear stress distribution in the composite slab resembles quite perfectly with the shear stress distribution in a NSC homogeneous slab thus, further agreeing with the above argument. Moreover, on studying the interface shear stresses in the composite section, there is no de-bonding observed ,i.e, shear stresses in the interface are well in limit (maximum shear stress around 0.88 at the time of diagonal shear failure), when compared with the analytical models as well. Numerical analyses performed on the composite slab specimen gives satisfactory results in accordance with these conditions, wherein, the load carrying capacity of the model with interface properties (as in the experiment) is slightly lower than the load carrying capacity in a model with perfect bond between the concrete layers. This is because, the interface is as strong as a perfect bond between the two concrete layers, thus, diagonal shear failure of the substrate is governing in all cases described in the case study. Considering all the discussions of this report, final conclusions are drawn, in the next chapter regarding the estimation of shear capacity of a composite concrete slab.

Conclusions and Recommendations

The report describes an analytical study performed to understand the shear behavior of a composite concrete slab with a validation of results using NLFEA with the help of ATENA software. The findings of this report explain the necessity and the nature of the finite element software, which is developed especially for reinforced concrete structures. The model thus explained is in accordance with the case study report of *Dr. Randl* [4]. For now, the report mainly concentrates on a specific case, where, a HSC overlay is applied on a RC slab. The results explain the stress distribution at the interface and the limiting values obtained from analytical models. Thus, this chapter includes the conclusions from these findings. Furthermore, some recommendations are prescribed in the end as prospective research topics.

6.1. CONCLUSIONS

- Homogeneous slabs with HSC (upper bound) and NSC (lower bound) properties pertaining to overlay and substrate layers respectively have been studied in previous sections and cracking pattern in each specimen is observed. Shear resistances are obtained using all shear models and a direct comparison is done with the experimental results. Values obtained using CSDT relate closely to the experimental results with lowest COV of 2.53%. Thus, the critical shear displacement theory gives a good estimate of shear capacity in case of composite concrete slabs.
- Among the two slab factor methods described, in the critical shear displacement theory, the method which uses actual wave parameters of amplitude and wave length gives a better estimation of shear resistance as compared to the approximate slab factor of 18.2 %. This is also because the actual calculation method considers the realistic crack pattern to calculate the change in shear displacement.
- From the cracking pattern obtained from CSDT, it can be concluded that the vertical cracks only propagate in the lower region, which is evidently the substrate region, if compared with the composite slab specimen. However, the vertical cracks later develop into a inclined critical crack which eventually reach the interface.
- Homogeneous slab with substrate concrete properties give good approximation of the shear behaviour for a composite concrete slab. By making changes to the limits in CSDT formulation according to the substrate thickness dimension, shear resistance for composite slab can be calculated.
- This is further validated with the load-displacement curve obtained for HSC and NSC homogeneous and composite concrete slabs. NSC homogeneous slab resembles the nature and failure criteria with the composite slab section. Both these curves exhibit brittle behavior whereas, the HSC homogeneous slab exhibits a ductile behavior. Furthermore, the shear stress at critical cross-sections complies with the argument thus giving similar values at the interface and at the critical section.
- In all cases, delamination of the interface does not occur. Diagonal shear failure is governing over the strength of interface. Maximum shear stress at the interface, once the shear span fails in diagonal shear, is 0.88. This is well in limit in case of the two limiting scenarios of perfect bond and no bond between the two concrete layers.

- Effect of bond between the two concrete layers is also studied. The interface properties in case of experimental set-up are as strong as a perfect bond condition. Hence, the nature of load - displacement curve in Figure 5.8, is very similar for perfect bond and bond with interface properties. Also, the load carrying capacities in both these cases do not differ significantly.
- The numerical results are compared with the experimental results to validate the numerical analysis. The maximum load carrying capacity in case of numerical model is slightly more than the experimental result. Also, the numerical model is a bit stiffer in the beginning which eventually leads to a higher value. The cracking pattern observed is also similar to the experimental crack pattern.

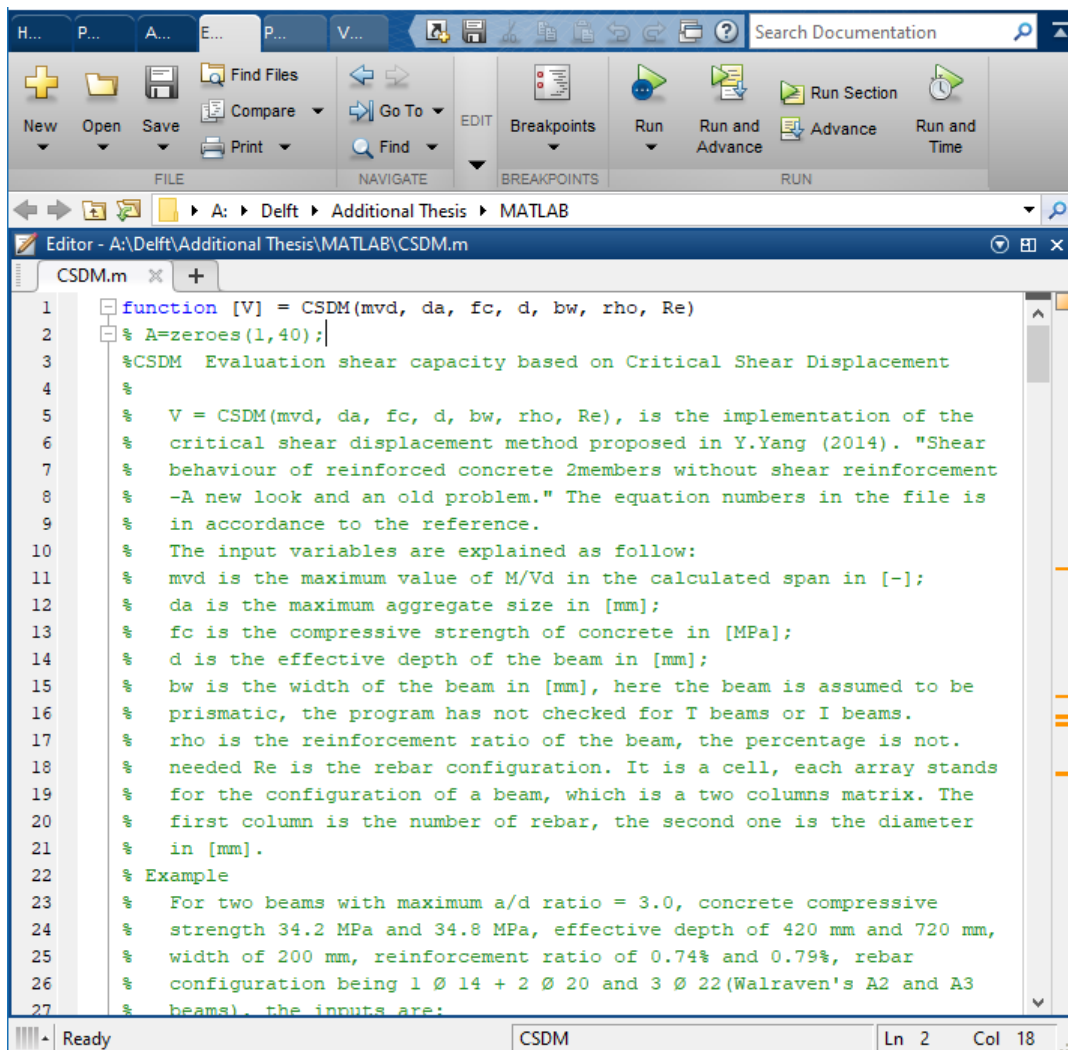
6.2. RECOMMENDATIONS

- The model is tested mainly for monotonic loading, further research can be done for fatigue/dynamic loading which will justify the loading pattern on a concrete bridge in real time.
- Changes in the overlay thickness can be incorporated to check for any changes in the shear behavior.
- A parametric study can be done further by varying the interface properties and studying the behavior of the composite slab.
- An improved numerical model based on the observations of this report can be tested. The results obtained might help in proper modelling of a composite concrete specimen, using ATENA FEM software.
- In ATENA Engineering 2D software, it is difficult to model a 'no connection' as the results obtained under this report's observations are not satisfactory for an 'uncoupled behavior' of the concrete layers. Only an analytical study was hence possible in this report regarding an uncoupled model.

A

CODE for Critical Shear Displacement Theory Method

To calculate the shear capacity using the critical shear displacement theory the following code needs to be run by using the input variables as shown in Table 3.7



```
1 function [V] = CSDM(mvd, da, fc, d, bw, rho, Re)
2 % A=zeros(1,40);
3 %CSDM Evaluation shear capacity based on Critical Shear Displacement
4 %
5 % V = CSDM(mvd, da, fc, d, bw, rho, Re), is the implementation of the
6 % critical shear displacement method proposed in Y.Yang (2014). "Shear
7 % behaviour of reinforced concrete 2members without shear reinforcement
8 % -A new look and an old problem." The equation numbers in the file is
9 % in accordance to the reference.
10 % The input variables are explained as follow:
11 % mvd is the maximum value of M/Vd in the calculated span in [-];
12 % da is the maximum aggregate size in [mm];
13 % fc is the compressive strength of concrete in [MPa];
14 % d is the effective depth of the beam in [mm];
15 % bw is the width of the beam in [mm], here the beam is assumed to be
16 % prismatic, the program has not checked for T beams or I beams.
17 % rho is the reinforcement ratio of the beam, the percentage is not.
18 % needed Re is the rebar configuration. It is a cell, each array stands
19 % for the configuration of a beam, which is a two columns matrix. The
20 % first column is the number of rebar, the second one is the diameter
21 % in [mm].
22 % Example
23 % For two beams with maximum a/d ratio = 3.0, concrete compressive
24 % strength 34.2 MPa and 34.8 MPa, effective depth of 420 mm and 720 mm,
25 % width of 200 mm, reinforcement ratio of 0.74% and 0.79%, rebar
26 % configuration being 1 Ø 14 + 2 Ø 20 and 3 Ø 22 (Walraven's A2 and A3
27 % beams). the inputs are:
```

```

CSDM.m x +
27 % beams), the inputs are:
28 % % %
29 % mvd = [3.96; 3];
30 % da = [32; 16];
31 % fc = [35; 34.8];
32 % d = [197; 720];
33 % bw = [1000; 200];
34 % rho = [.03; .0079];
35 % Re = {[10 26];[3 22]};
36 % V = CSDM(mvd, da, fc, d, bw, rho, Re);
37
38 %
39 %Last modified by Yuguang Yang on April 04 2014. Copy right reserved.
40
41 % CoreNum = 4; % when parallel calculation is available on the computer,
42 % determine the number of cores that is available
43 global Es Ec
44
45 Es = 210000; % elastic modules of steel in MPa
46 Ec = 25470; % elastic modules of concrete in MPa, only effecting the
47 %Ec = 22000*((fc/10)^0.3);
48 % crack height calculation, thus a rough estimation is sufficient.
49 % validation, it is recommended to make Ra = 0.75 for LWA concrete;
50 % and keep Ra = 1.0, while reduce fc back to 60 MPa for HSC
51 n = numel(d); % number of tests
52 As = rho.*bw.*d; % reinforcement area
53 Ra = ones(n,1);

```

```

CSDM.m x +
52 As = rho.*bw.*d; % reinforcement area
53 Ra = ones(n,1);
54 % A = zeros(1, 40);%reduction factor for special concrete types such as
55 % HSC or LWA concrete.
56 br = zeros(n,1);D = br;
57 if nargin > 6
58 for l = 1:n
59 br(l) = sum(Re{l}(:,1).*Re{l}(:,2)); % the part of width occupied
60 % by rebar for dowel force Vdw calculation (only applicable when
61 % all the rebars are in one layer)
62 D(l) = sum(Re{l}(:,1).*Re{l}(:,2).^2)/sum(Re{l}(:,1).*Re{l}(:,2));
63 % equivalent rebar diameter Deff, calculated with eq..(4.16)
64 end
65 else
66 % When rebar configuration is not available, assuming there are four
67 % bars in one layer, calculate the rebar diameter accordingly.
68 Re = ones(n,1)*[4 4];
69 Re(2) = (As/pi).^5;
70 br = 4*Re(:,2); D = Re(:,2);
71 end
72 Vdw = V_dw(bw, br, fc, D); % calculate the contribution of dowel action
73 V = zeros(n,1);
74
75 %Initialize Matlab Parallel Computing Environment
76 % if parpool('local')<=0 % check parallel computing environment
77 % parpool('open','local',CoreNum);
78 % start parallel computing environment

```

```

CSDM.m x +
77 % parpool('open','local',CoreNum);
78 % start parallel computing environment
79 % end
80
81 - for l = 1:n
82     V(l) = Vm(mvd(l), da(l), fc(l), d(l), bw(l), As(l), Vdw(l), ...
83         rho(l), D(l), Ra(l));
84     % calculation of the maximum shear resistance of each tests
85 -end
86 % parpool close
87 -end
88 %-----
89 - function V = Vm(mvd, da, fc, d, bw, As, Vdw, rho, D, Ra)
90
91     global Es Ec
92
93     ne = Es/Ec; % ratio between Es and Ec for crack height calculation
94     delta = min((3.267e-5.*d*25/D+.002204), .025);
95     scr = (1+rho.*ne-(2*rho.*ne+(rho.*ne).^2).^5).^5.*d; % major crack height
96     lcrm = scr./1.28; % average crack spacing of major cracks
97     z = (2*d + scr)/3; % internal level arm
98     V1 = 1.5*d*bw; % first guess of shear resistance
99     V0 = 0; count = 0; % initiation of iteration
100
101 - while abs(V0-V1) > 10
102     M0 = V1*d*mvd; % cross sectional moment

```

```

CSDM.m x +
101 - while abs(V0-V1) > 10
102     M0 = V1*d*mvd; % cross sectional moment
103     w = M0/z/As/Es*lcrm; % estimation of average crack width eq..(4.8)
104     V0 = V1;
105
106     Vai = V_ai(delta, w, da, scr, fc, bw); % aggregate interlock
107     Vc = V_c(z,d, V0); % shear force in compression zone
108     V1 = Ra*Vai + Vc + Vdw; % summation of total shear force
109
110     V = V1;
111
112     if count == 20 % maximum iteration number is 20
113         break
114     end
115     count = count+1;
116 -end
117     mvd0 = 2;
118     if mvd < 2
119         V = V*2/mvd0;
120     end
121     m = [V1; Vai; Vc; Vdw]
122     % fctm = (fc<58).*3.*(fc-8).^2/3+(fc>=58).*2.12.*log(1+(fc/10));
123 -end
124
125 %-----
126 - function Vai = V ai(delta, w, da, scr, fc, bw)

```

```

125 %-----
126 function Vai = V_ai(delta, w, da, scr, fc, bw)
127 % shear resistance contributed by aggregate interlock, based on eq..(4.4)
128 w0 = 0.01; % crack width at crack tipD
129 dw = (w0-w)/100; % increment of crack width in the linear crack profile
130 CrackProfile = (w: dw: w0); % crack profile, divided into 100 sections
131 n = numel(CrackProfile);
132 L = scr/n;
133 fc = min(fc,60); % limitation for high strength concrete
134 tau = zeros(size(CrackProfile));
135 parfor l = 1:n
136     [~,tau(l)]=AI_walraven(CrackProfile(l), delta, da, fc);
137     % Walraven's aggregate interlocking formula eq..(3.30)
138 end
139 Vai = -sum(tau.*L)*bw;
140 % A[1:n]=[l, Vai];
141 % disp(a);
142 % alternative simplified AI formula: eq..(4.7), much faster than
143 % Walraven's formula:
144 % Vai = (-978*delta.^2+85*delta-.27).*fc.^56.*bw.*.03./(w-.01).*scr;
145 end
146 %
147 %-----
148 function Vdw = V_dw(bw, br, fc, D)
149 % maximum dowel action force, based on eq..(3.28)
150 Vdw = 1.64*(bw-br).*D.*(fc).^33;

```

```

150 Vdw = 1.64*(bw-br).*D.*(fc).^33;
151 end
152 %-----
153 function Vc = V_c(z, d, V)
154 % shear force contrition in compression zone, based on eq..(3.26)
155 Vc = 2*(d-z)/z*V;
156 end
157 %=====
158 function [sig,tau]=AI_walraven(w0, D0, da, fc)
159 %AI_Walraven Walraven's formula for aggregate interlock eq..(3.30)
160 % [sig,tau]=AI_walraven(w0, D0, da, fc), calculated the shear and
161 % normal stresses [MPa] generated due to aggregate interlock when the
162 % normal or shear displacement at the crack faces is given. The
163 % function only allows the input of single values. If you have an array
164 % please do it through iteration. This function has to be a separate
165 % file named 'AI_walraven.m'. The inputs of the function are:
166 % normal crack opening w0 [mm],
167 % shear crack opening D0 [mm],
168 % maximum aggregate size da [mm],
169 % concrete compressive strength fc [MPa].
170 %Exmample
171 % [sig,tau]=AI_walraven(0.01,0.02,16,34.2);
172
173 %Last modified by Yuguang Yang on April 04 2014. Copy right reserved.
174
175 global dm pk u w D

```

```

CSDM.m x +
175 - global dm pk u w D
176 - w = w0*(w0>0); % normal crack opening
177 - D = abs(D0); % shear crack opening
178 - dm = da; % maximum aggregate size
179 - % situation when there is no contact between crack faces
180 - if w > dm
181 -     sig = 0;
182 -     tau = 0;
183 - % situation when the shear displacement is larger than Dmax
184 - else if D > dm
185 -     [sig,tau]=AI_walraven_u(w0, da, fc);
186 -     else
187 - % normal situation
188 - pk = 0.75;
189 - u = .4; % friction coefficient
190 - fcc = fc;
191 - sig_pu = 6.39*fcc^(.56); % crush strength of the cement matrix
192 - if D > w
193 -     Ay = quad(@ay,2*w,dm);
194 -     Ax = quad(@ax,2*w,dm);
195 - else
196 -     if (w^2+D^2)/D<dm
197 -     Ay = quad(@ay,(w^2+D^2)/D,dm);
198 -     Ax = quad(@ax,(w^2+D^2)/D,dm);
199 -     else

```

```

CSDM.m x +
199 -     else
200 -     Ay = 0;
201 -     Ax = 0;
202 -     end
203 - end
204 - sig = sig_pu*(Ax-u*Ay);
205 - tau = sig_pu*(Ay+u*Ax)*(-D/D0);
206 - end
207 - end
208 - end
209 - function [sig,tau]=AI_walraven_u(w0)
210 - % Walraven's formula when the shear displacement is larger than Dmax
211 - % aggregate size.
212 - global dm pk u w
213 - w = w0; % crack opening [mm]
214 - dm = 16; % maximum aggregate size [mm]
215 - pk = 0.75; % percentage of aggregate
216 - u = .4; % friction
217 - fcc = 40; % concrete compressive strength [MPa]
218 - sig_pu = 6.39*fcc^(.56); % yield strength of concrete under three
219 - % dimensional loading
220 - if w^2 < dm
221 - Ay = quad(@ayu,2*w,dm);
222 - Ax = quad(@axu,2*w,dm);
223 - sig = sig_pu*(Ax-u*Ay);

```

```

CSDM.m x +
223 - sig = sig_pu*(Ax-u*Ay);
224 - tau = sig_pu*(Ay+u*Ax);
225 - else
226 - sig = 0;
227 - tau = 0;
228 - end
229 - end
230 - function [F] = F(d0,dm)
231 - % aggregate size distribution function F(D), see eq..(3.30)
232 - d = d0/dm;
233 - F = .532*d.^5-.212*d.^4-.072*d.^6-.036*d.^8-.025.^10;
234 - end
235 - function [G1] = G1(d,D,w)
236 - % function G1(n,t,D), see eq..(3.30)
237 - um = UM(w,D,d);
238 - G1 = d.^(-3).*((d.^2-(w^2+D.^2)).^5.*D./(w^2+D.^2).^5.*um-w.*um-um.^2);
239 - end
240 - function [G2] = G2(d,D,w)
241 - % function G2(n,t,D), see eq..(3.30)
242 - um = UM(w,D,d);
243 - G2 = d.^(-3).*((D-(d.^2-w^2-D.^2).^5*w./(w^2+D.^2).^5.*um +...
244 - (um+w).*(d.^2/4-(w+um).^2).^5 - w*(d.^2/4-w^2).^5)+...
245 - d.^2/4.*asin((w+um)./d*2) - d.^2/4.*asin(2*w./d));
246 - end
247 - function [G3] = G3(d,w)

```

```

CSDM.m x +
247 - function [G3] = G3(d,w)
248 - % function G3(n,t,D), see eq..(3.30)
249 - G3 = d.^(-3).*(d/2-w).^2;
250 - end
251 - function [G4] = G4(d,w)
252 - % function G4(n,t,D), see eq..(3.30)
253 - G4 = d.^(-3).*(d.^2*pi/8-w*(d.^2/4-w^2).^5-d.^2/4.*asin(2*w./d));
254 - end
255 - function um = UM(w,D,d)
256 - % calculation of umax in G1 and G2
257 - um = (-w/2*(w^2+D^2)+(w^2*(w^2+D^2)^2-(w^2+D^2)*(w^2+D^2)^2- ...
258 - D^2*d.^2).^5/2)/(w^2+D^2);
259 - end
260 - function [ay] = ay(d)
261 - % projected contact area Ax in x direction in eq..(3.30)
262 - global dm pk w D
263 - if D > w
264 -     if w == 0
265 -         D0 = dm;
266 -     else
267 -         D0 = (w^2+D^2)/w;
268 -     end
269 -     d1 = d(d <= D0);
270 -     ay1 = pk*4/pi.*F(d1,dm).*G3(d1,w);
271 -     d2 = d(d > D0);

```

```

CSDM.m x +
271 - d2 = d(d > D0);
272 - ay2 = pk*4/pi.*F(d2, dm).*G1(d2, D, w);
273 - ay = [ay1, ay2];
274 - else
275 -     ay = pk*4/pi.*F(d, dm).*G1(d, D, w);
276 - end
277 - end
278 - function [ax] = ax(d)
279 -     % projected contact area Ax in x direction in eq..(3.30)
280 -     global dm pk w D
281 -     if D > w
282 -         if w == 0
283 -             D0 = dm;
284 -         else
285 -             D0 = (w^2+D^2)/w;
286 -         end
287 -         d1 = d(d <= D0);
288 -         ax1 = pk*4/pi.*F(d1, dm).*G4(d1, w);
289 -         d2 = d(d > D0);
290 -         ax2 = pk*4/pi.*F(d2, dm).*G2(d2, D, w);
291 -         ax = [ax1, ax2];
292 -     else
293 -         ax = pk*4/pi.*F(d, dm).*G2(d, D, w);
294 -     end
295 - end

```

```

CSDM.m x +
283 -     D0 = dm;
284 -     else
285 -         D0 = (w^2+D^2)/w;
286 -     end
287 -     d1 = d(d <= D0);
288 -     ax1 = pk*4/pi.*F(d1, dm).*G4(d1, w);
289 -     d2 = d(d > D0);
290 -     ax2 = pk*4/pi.*F(d2, dm).*G2(d2, D, w);
291 -     ax = [ax1, ax2];
292 - else
293 -     ax = pk*4/pi.*F(d, dm).*G2(d, D, w);
294 - end
295 - end
296 - function [ay] = ayu(d)
297 -     % projected contact area Ay in y direction when the shear displacement is
298 -     % larger than maximum aggregate size D > dm
299 -     global dm pk w
300 -     ay = pk*4/pi.*F(d, dm).*G3(d, w);
301 - end
302 - function [ax] = axu(d)
303 -     % projected contact area Ax in x direction when the shear displacement is
304 -     % larger than maximum aggregate size D > dm
305 -     global dm pk w
306 -     ax = pk*4/pi.*F(d, dm).*G4(d, w);
307 - end
308 -

```


B

Excel calculation sheets

Following section contains all the excel calculation sheets used for the completion of this additional thesis report.

Slab no.		$f_{cubes150}$ [Mpa]	$f_{cylinder}$ [Mpa]	$f_{c1} +$ [Mpa]	modulus of elasticity [Mpa]	Roughness (mm)	Topping	Last Maximum (kN)	F (kN)	delta (mm)	lcm (mm)	MO (kN-m)	scr (mm)	V (kN)	Vai (kN)	Vc (kN)	Vdv (kN)	factor deviation	NSC	HSC
1	substrate	62.09	50.63	5.05	28390	1.6	NSC	902.40	451.20	0.0103	116.30	315.354	148.86	404.300	157.170	131.910	115.210	1.116	11.60%	0.00%
	overlay	50.47	41.16	4.49	25470		NSC	902.40	451.20	0.0103	112.90	300.217	144.51	384.900	145.800	131.490	107.600	1.172	17.23%	0.00%
2	substrate	61.80	50.40	5.04	28640	3	HSC	951.30	475.65	0.0103	116.57	314.631	149.21	403.370	157.210	131.120	115.040	1.179	0.00%	17.92%
	overlay	88.40	72.09	5.52	36510		HSC	951.30	475.65	0.0103	123.89	328.775	158.58	421.510	168.690	123.360	129.460	1.128	0.00%	12.84%
3	substrate	61.96	50.53	5.04	28390	3	NSC	914.10	457.05	0.0103	116.30	315.169	148.86	404.060	157.090	131.830	115.140	1.131	13.11%	0.00%
	overlay	49.79	40.60	4.46	25470		NSC	914.10	457.05	0.0103	112.90	299.004	144.51	383.340	145.260	130.960	107.120	1.192	19.23%	0.00%
4	substrate	61.74	50.35	5.03	28390	0.8	NSC	914.10	457.05	0.0103	116.30	314.836	148.86	403.640	156.940	131.690	115.000	1.168	16.76%	0.00%
	overlay	47.30	38.57	4.34	25470		NSC	942.60	471.30	0.0103	112.90	294.505	144.51	377.570	143.260	128.990	105.320	1.248	24.82%	0.00%
5	substrate	59.48	48.51	4.93	28640	1.5	HSC	951.90	475.95	0.0103	116.57	311.087	149.21	398.830	155.590	129.640	113.600	1.193	0.00%	19.34%
	overlay	97.59	79.59	5.72	36510		HSC	951.90	475.95	0.0103	123.89	331.851	158.58	425.460	167.180	124.510	133.760	1.119	0.00%	11.87%
6	substrate	49.01	39.97	4.42	28640	1.7	HSC	896.70	448.35	0.0103	116.57	293.758	149.21	376.620	147.630	122.420	106.570	1.150	0.00%	19.05%
	overlay	101.79	83.01	5.82	37450		HSC	896.70	448.35	0.0103	124.64	332.391	159.53	426.150	167.180	123.330	135.630	1.052	0.00%	5.21%
7	substrate	66.86	54.52	5.28	28640	0.8	HSC	1014.90	507.45	0.0103	116.57	322.048	149.21	412.880	160.610	134.210	118.060	1.229	0.00%	22.90%
	overlay	93.27	76.06	5.63	36510		HSC	1014.90	507.45	0.0103	123.89	330.426	158.58	423.630	167.880	123.980	131.770	1.158	0.00%	19.79%
8	substrate	57.28	46.71	4.82	28990	0.8	HSC	947.20	473.60	0.0103	116.95	307.222	149.69	393.880	154.320	127.370	112.190	1.202	0.00%	20.24%
	overlay	98.79	80.56	5.75	37450		HSC	947.20	473.60	0.0103	124.64	331.436	159.53	424.920	167.650	122.980	134.300	1.115	0.00%	11.46%
											124.64		159.53						17.13%	16.06%

Figure B.1: Calculation of various parameters according to CSDT using MATLAB code in A

Fck	Cylinder	12	16	20	25	30	35	40	45	50	55	60	70	80	90	50,60
Fck	Cube	15	20	25	30	37	45	50	55	60	67	75	85	95	105	62,09
		1.25	1.25	1.25	1.20	1.23	1.29	1.25	1.22	1.20	1.22	1.25	1.21	1.19	1.17	1.23
		0.80	0.80	0.80	0.83	0.81	0.78	0.80	0.82	0.83	0.82	0.80	0.82	0.84	0.86	0.82

Figure B.2: Relation between $f_{c,cube}$ and $f_{c,cylinder}$ according to Eurocode

Eurocode shear strength				F	V	fcm	Ec	Vr	LB	UB	Average	Avg/V	SD	
fk	35 Mpa	γc	1.5	902.40	451.20	50.63	28390	255.109	234.62	255.11	244.87	45.73%	0.54	0.00031
fd	23.33 Mpa			902.40	451.20	41.16	25470	234.624	234.62	255.11	244.87	45.73%	0.54	0.00031
d	257 mm			951.30	475.65	50.40	28640	254.637	254.64	292.20	273.42	42.52%	0.57	0.00021
b	1000 mm			951.30	475.65	72.09	36510	292.198	254.64	292.20	273.42	42.52%	0.57	0.00021
ρho	0.02 (-)			914.10	457.05	50.53	28390	254.898	233.31	254.90	244.10	46.59%	0.53	0.00069
Crd/c	0.12			942.60	471.30	50.35	28390	254.539	228.37	254.54	241.45	48.77%	0.51	0.00230
αcp	0.00 Mpa	Ned/Ac		942.60	471.30	38.57	25470	228.368	228.37	254.54	241.45	48.77%	0.51	0.00230
k	1.882162			951.90	475.95	48.51	28640	250.796	250.80	303.16	276.98	41.81%	0.58	0.00047
k1	0.15			951.90	475.95	79.59	36510	303.159	250.80	303.16	276.98	41.81%	0.58	0.00047
Vrd,c	238.89 kN			896.70	448.35	39.97	28640	231.785	231.78	307.91	269.85	39.81%	0.60	0.00173
				896.70	448.35	83.01	37450	307.914	231.78	307.91	269.85	39.81%	0.60	0.00173
				1014.90	507.45	54.52	28640	262.636	262.64	298.11	280.37	44.75%	0.55	0.00006
				1014.90	507.45	76.06	36510	298.107	262.64	298.11	280.37	44.75%	0.55	0.00006
vmin	0.535 Mpa			947.20	473.60	46.71	28990	247.040	247.04	304.53	275.79	41.77%	0.58	0.00048
Vrd,c min	137.41 kN			947.20	473.60	80.56	37450	304.533	247.04	304.53	275.79	41.77%	0.58	0.00048
				Mean	470.07				Mean	263.35		43.97%	0.56	0.02796
												42.13%		4.99% COV

Figure B.3: Shear force calculations using Eurocode2

F	V	M	a	d	rho	F	V	fcm	Ec	c	eps	Vr	LB	UB	Average	Avg./V	SD
952	476	371.28	780	257	0.02	902.40	451.20	50.63	28390	115.84	0.000325	504.39	461.27	504.39	482.83	7.01%	0.00121
dg	32 mm					902.40	451.20	41.16	25470	120.33	0.000298	461.27	461.27	504.39	482.83	7.01%	0.00121
b	1000 mm					951.30	475.65	50.40	28640	115.48	0.000344	497.99	497.99	579.46	538.72	13.26%	0.00077
fc	35 Mpa					951.30	475.65	72.09	36510	105.74	0.000397	579.46	497.99	579.46	538.72	13.26%	0.00077
fcm	43 Mpa					914.10	457.05	50.53	28390	115.84	0.000329	502.74	457.20	502.74	479.97	5.01%	0.00300
Ec	32672 Mpa					914.10	457.05	40.60	25470	120.33	0.000302	457.20	457.20	502.74	479.97	5.01%	0.00300
Es	210000 Mpa					942.60	471.30	50.35	28390	115.84	0.000339	499.13	443.37	499.13	471.25	0.01%	0.01103
c	110.1362 mm					942.60	471.30	38.57	25470	120.33	0.000311	443.37	443.37	499.13	471.25	0.01%	0.01103
eps	0.000375 (-)					951.90	475.95	48.51	28640	115.48	0.000345	488.50	488.50	608.75	548.63	15.27%	0.00228
Vr	408.4541 kN					951.90	475.95	79.59	36510	105.74	0.000398	608.75	488.50	608.75	548.63	15.27%	0.00228
						896.70	448.35	39.97	28640	115.48	0.000325	448.13	448.13	627.64	537.89	19.97%	0.00898
variation	14.19%					896.70	448.35	83.01	37450	104.74	0.000379	627.64	448.13	627.64	537.89	19.97%	0.00898
						1014.90	507.45	54.52	28640	115.48	0.000367	511.78	511.78	587.22	549.50	8.29%	0.00049
						1014.90	507.45	76.06	36510	105.74	0.000424	587.22	511.78	587.22	549.50	8.29%	0.00049
						369.408	947.20	473.60	46.71	28990	114.98	0.000346	479.07	611.57	545.32	15.14%	0.00216
						947.20	473.60	80.56	37450	104.74	0.000400	611.57	479.07	611.57	545.32	15.14%	0.00216
														Mean	519.26	10.50%	0.06116
																14.39%	5.54% COV

Figure B.4: Shear force calculations using Critical Shear Crack Theory

Slab no.	Concrete [Mpa]	f _{c,calc}	modulus of elasticity [MPa]	Roughness (mm)	Excluding Slab Factor			Including Slab Factor			Excluding Slab Factor			Including Slab Factor			Including Slab Factor 28.2%				
					V ₁ (kN)	Val ₁ (kN)	Vc ₁ (kN)	Vd _{w,1} (kN)	V ₂ (kN)	Val ₂ (kN)	Vc ₂ (kN)	Vd _{w,2} (kN)	LB ₁ (kN)	UB ₁ (kN)	AVG ₁ (kN)	LB ₂ (kN)	UB ₂ (kN)	AVG ₂ (kN)	LB ₃ (kN)	UB ₃ (kN)	AVG ₃ (kN)
1	substrate	50.63	5.05	28990	404.30	157.17	131.91	115.21	428.45	173.45	139.79	115.21	384.90	404.30	394.60	407.88	428.45	416.17	454.95	477.88	466.42
	overlay	41.16	4.49	25470	384.90	145.80	131.49	107.60	407.88	160.93	139.35	107.60	384.90	404.30	394.60	407.88	428.45	416.17	454.95	477.88	466.42
2	substrate	50.40	5.04	28640	403.37	157.21	131.12	115.04	427.48	173.49	138.95	115.04	403.37	421.51	412.44	427.48	446.32	436.90	476.78	498.22	487.50
	overlay	72.09	5.52	36510	421.51	168.69	123.36	129.46	446.32	186.24	130.62	129.46	403.37	421.51	412.44	427.48	446.32	436.90	476.78	498.22	487.50
3	substrate	50.33	5.04	28990	404.06	157.09	131.83	115.14	428.20	173.35	139.71	115.14	383.34	404.06	393.70	406.24	428.20	417.22	453.11	477.60	465.35
	overlay	40.60	4.46	25470	383.34	145.26	130.96	107.12	406.24	160.33	138.79	107.12	383.34	404.06	393.70	406.24	428.20	417.22	453.11	477.60	465.35
4	substrate	50.35	5.03	28990	403.64	156.94	131.69	115.00	427.75	173.18	139.56	115.00	377.57	403.64	390.61	400.14	427.75	413.95	446.29	477.10	461.70
	overlay	38.57	4.34	25470	377.57	143.26	128.99	105.32	400.14	158.12	136.70	105.32	377.57	403.64	390.61	400.14	427.75	413.95	446.29	477.10	461.70
5	substrate	48.51	4.93	28640	398.83	155.59	129.64	113.60	422.68	171.69	137.39	113.60	398.83	425.46	412.15	422.68	450.20	436.64	471.42	502.89	487.16
	overlay	79.59	5.72	36510	425.46	167.18	124.51	133.76	450.20	184.68	131.75	133.76	398.83	425.46	412.15	422.68	450.20	436.64	471.42	502.89	487.16
6	substrate	39.97	4.42	28640	376.62	147.63	122.42	106.57	399.24	162.90	129.77	106.57	376.62	426.15	401.39	399.24	450.83	425.04	445.16	503.71	474.44
	overlay	83.01	5.82	37450	426.15	167.18	123.33	135.63	450.83	184.72	130.48	135.63	376.62	426.15	401.39	399.24	450.83	425.04	445.16	503.71	474.44
7	substrate	54.52	5.28	28640	412.88	160.61	134.21	118.06	437.51	177.23	142.21	118.06	412.88	423.63	418.26	437.51	448.40	442.96	488.02	500.73	494.38
	overlay	76.06	5.63	36510	423.63	167.88	123.98	131.77	448.40	185.40	131.23	131.77	412.88	423.63	418.26	437.51	448.40	442.96	488.02	500.73	494.38
8	substrate	46.71	4.82	28990	393.88	154.32	127.37	112.19	417.47	170.28	134.99	112.19	393.88	424.92	409.40	417.47	449.62	433.55	465.57	502.26	483.91
	overlay	80.56	5.75	37450	424.92	167.65	122.98	134.30	449.62	185.20	130.13	134.30	393.88	424.92	409.40	417.47	449.62	433.55	465.57	502.26	483.91
													Mean	404.07		Mean	428.03		Mean	477.61	

Figure B.7: Comparison of shear force obtained using CSDT (excluding slab factor, including actual slab factor and including estimated slab factor)-1

Slab no.	substrate overlay	$f_{c,expt}$ [Mpa]	$f_{c,calc}$	modulus of elasticity [MPa]	Roughness (mm)	Variation			Variation		
						AVG 1/V	AVG 2/V	AVG 3/V	IV-AVG 1/V	IV-AVG 2/V	IV-AVG 3/V
1	substrate	50.63	5.05	28390	1.6	0.87	0.93	1.03	12.54%	7.32%	9.37%
	overlay	41.16	4.49	25470		0.87	0.93	1.03	12.54%	7.32%	9.37%
2	substrate	50.40	5.04	28640	3	0.87	0.92	1.02	13.29%	8.15%	2.49%
	overlay	72.09	5.52	36510		0.87	0.92	1.02	13.29%	8.15%	2.49%
3	substrate	50.33	5.04	28390	3	0.86	0.91	1.02	13.86%	8.71%	1.82%
	overlay	40.60	4.46	25470		0.86	0.91	1.02	13.86%	8.71%	1.82%
4	substrate	50.35	5.03	28390	0.8	0.83	0.88	0.98	17.12%	12.17%	2.04%
	overlay	38.57	4.34	25470		0.83	0.88	0.98	17.12%	12.17%	2.04%
5	substrate	48.51	4.93	28640	1.5	0.87	0.92	1.02	13.41%	8.30%	2.35%
	overlay	79.39	5.72	36510		0.87	0.92	1.02	13.41%	8.30%	2.35%
6	substrate	39.97	4.42	28640	1.7	0.90	0.95	1.06	10.48%	5.20%	5.82%
	overlay	83.01	5.82	37450		0.90	0.95	1.06	10.48%	5.20%	5.82%
7	substrate	54.52	5.28	28640	0.8	0.82	0.87	0.97	17.58%	12.71%	2.58%
	overlay	76.06	5.63	36510		0.82	0.87	0.97	17.58%	12.71%	2.58%
8	substrate	46.71	4.82	28390	0.8	0.86	0.92	1.02	13.56%	8.46%	2.18%
	overlay	80.36	5.75	37450		0.86	0.92	1.02	13.56%	8.46%	2.18%
						0.86	0.91	1.02	13.98%	8.88%	2.83%

Figure B.8: Comparison of shear force obtained using CSDT (excluding slab factor, including actual slab factor and including estimated slab factor)-2

SN		EC		CSCT		CSDT (w/o sf)		CSDT (w/ sf_act)		CSDT (w/ sf_est)	
		V /V	SD	V /V	SD	V /V	SD	V /V	SD	V /V	SD
1	0.54	0.000311	1.07	0.001213	0.87	0.000206	0.93	0.000242	1.03	0.000287	
2	0.57	0.000210	1.13	0.000766	0.87	0.000048	0.92	0.000053	1.02	0.000066	
3	0.53	0.000688	1.05	0.003001	0.86	0.000001	0.91	0.000003	1.02	0.000002	
4	0.51	0.002305	1.00	0.011031	0.83	0.000988	0.88	0.001084	0.98	0.001380	
5	0.58	0.000468	1.15	0.002281	0.87	0.000033	0.92	0.000033	1.02	0.000046	
6	0.60	0.001726	1.20	0.008981	0.90	0.001228	0.95	0.001352	1.06	0.001715	
7	0.55	0.000061	1.08	0.000487	0.82	0.001295	0.87	0.001466	0.97	0.001809	
8	0.58	0.000494	1.15	0.002163	0.86	0.000018	0.92	0.000018	1.02	0.000025	
=>	0.56	0.02796	1.10	0.06116	0.86	0.02184	0.91	0.02306	1.02	0.02581	
COV		4.99%		5.54%		2.54%		2.53%		2.54%	

Figure B.9: Calculation of coefficients of variation for all three shear models

L	3600 mm				
a	780 mm				
d	257 mm				
	I (mm)	b (mm)	h (mm)	C ₀ (mm) from bot.	I (mm ⁴)
Substrate	3600	1000	240	120	1152000000
overlay	3600	1000	60	270	180000000
Combined	3600	1000	300	150	2250000000

Figure B.10: RC slab and HSC overlay dimensions as separate and combined elements

2 Coupled behaviour		Ely(AI+E2)2AZ; yI=(h-2)y2=(270-h)		Ely(AI+E1)E1H+E2I2I		E2y E2/E1H+E2I2I		27.47988																		
Slab no.		Topping	Last Maximum m (kN)	M (kN-m) at centroid section (exp.)	E (MPa)	ELI (Nmm ²)	EAI	n (E2A2/E1 A1)	h (mm) from bottom	ei	ei	ei	ei	ei	ei	ei										
1	substrate	N5C	902.40	451.20	28390	3.7850E+13	6.8E+09	0.22	117.48	24.06	-15.09	24.06	-15.09	-13.54	-15.09	-13.54	-22.32	0	0.0008	-5E-04	0.0000	0.0008	-0.0005	-0.0005	-0.0009	0.0
	overlay	N5C	902.40	451.20	25470	2.3399E+13	1.5E+09	0.22	117.48	-13.54	-22.32	-13.54	-22.32	0	0	240	240	300	300	-5E-04	-9E-04	0	0	240	240	300
2	substrate	N5C	951.30	475.65	28640	4.2026E+13	6.9E+09	0.32	156.25	23.39	-12.53	23.39	-12.53	-15.97	-12.53	-15.97	-27.41	0	0.0009	-4E-04	0.0000	0.0008	-0.0004	-0.0004	-0.0008	0.0
	overlay	N5C	951.30	475.65	36510	2.9001E+13	2.2E+09	0.32	156.25	-15.97	-27.41	-15.97	-27.41	0	0	240	240	300	300	-4E-04	-8E-04	0	0	240	240	300
3	substrate	N5C	916.70	457.05	28390	3.7850E+13	6.8E+09	0.22	117.48	24.37	-15.29	24.37	-15.29	-13.72	-15.29	-13.72	-22.61	0	0.0009	-5E-04	0.0000	0.0009	-0.0005	-0.0005	-0.0009	0.0
	overlay	N5C	916.70	457.05	25470	2.3399E+13	1.5E+09	0.22	117.48	-13.72	-22.61	-13.72	-22.61	0	0	240	240	300	300	-5E-04	-9E-04	0	0	240	240	300
4	substrate	N5C	942.60	471.30	28390	3.7850E+13	6.8E+09	0.22	117.48	25.13	-15.77	25.13	-15.77	-14.14	-15.77	-14.14	-23.32	0	0.0009	-6E-04	0.0000	0.0009	-0.0006	-0.0006	-0.0009	0.0
	overlay	N5C	942.60	471.30	25470	2.3399E+13	1.5E+09	0.22	117.48	-14.14	-23.32	-14.14	-23.32	0	0	240	240	300	300	-6E-04	-9E-04	0	0	240	240	300
5	substrate	N5C	951.30	475.65	28640	4.2026E+13	6.9E+09	0.32	156.25	23.39	-12.54	23.39	-12.54	-15.96	-12.54	-15.96	-27.43	0	0.0008	-4E-04	0.0000	0.0008	-0.0004	-0.0004	-0.0008	0.0
	overlay	N5C	951.30	475.65	371241	2.9001E+13	2.2E+09	0.32	156.25	-15.96	-27.43	-15.96	-27.43	0	0	240	240	300	300	-4E-04	-8E-04	0	0	240	240	300
6	substrate	N5C	856.70	443.35	28640	4.2026E+13	6.9E+09	0.32	156.95	21.90	-11.59	21.90	-11.59	-15.15	-11.59	-15.15	-26.10	0	0.0008	-4E-04	0.0000	0.0008	-0.0004	-0.0004	-0.0007	0.0
	overlay	N5C	856.70	443.35	349.713	2.9399E+13	2.2E+09	0.33	156.95	-15.15	-26.10	-15.15	-26.10	0	0	240	240	300	300	-4E-04	-7E-04	0	0	240	240	300
7	substrate	N5C	1014.90	507.45	28640	4.2026E+13	6.9E+09	0.32	156.25	24.94	-13.37	24.94	-13.37	-17.04	-13.37	-17.04	-29.25	0	0.0009	-5E-04	0.0000	0.0009	-0.0005	-0.0005	-0.0008	0.0
	overlay	N5C	1014.90	507.45	395.811	2.9001E+13	2.2E+09	0.32	156.25	-17.04	-29.25	-17.04	-29.25	0	0	240	240	300	300	-5E-04	-8E-04	0	0	240	240	300
8	substrate	N5C	947.20	473.60	28990	4.2726E+13	7E+09	0.32	156.62	23.20	-12.35	23.20	-12.35	-15.96	-12.35	-15.96	-27.44	0	0.0008	-4E-04	0.0000	0.0008	-0.0004	-0.0004	-0.0007	0.0
	overlay	N5C	947.20	473.60	365.408	2.9516E+13	2.2E+09	0.32	156.62	-15.96	-27.44	-15.96	-27.44	0	0	240	240	300	300	-4E-04	-7E-04	0	0	240	240	300

Figure B.12: Normal stress calculation along the cross-section of coupled members

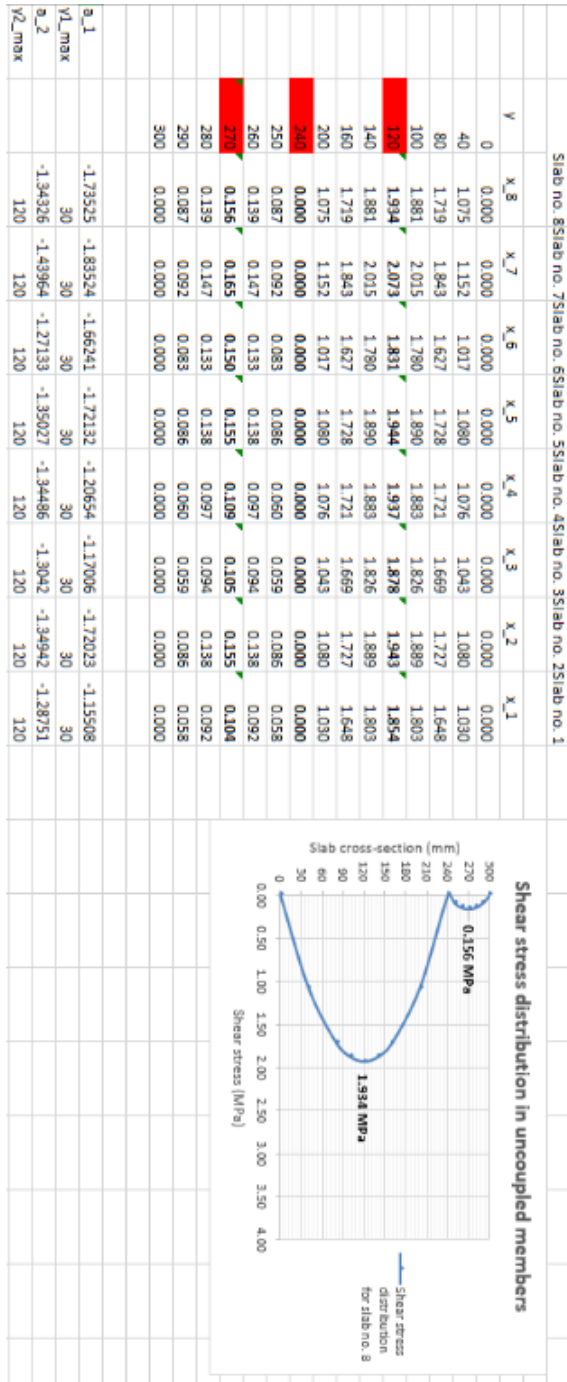


Figure B.13: Shear stress calculation along the cross-section of uncoupled members

Coupled Members									
	Slab no. 8	Slab no. 7	Slab no. 6	Slab no. 5	Slab no. 4	Slab no. 3	Slab no. 2	Slab no. 1	
d	257	257	257	257	257	257	257	257	mm
a	780	780	780	780	780	780	780	780	mm
NA	156.62	156.25	156.95	156.25	147.48	147.48	156.25	147.48	mm
f _c	46.71	54.52	39.97	48.51	50.35	50.53	50.40	50.63	MPa
rho	0.0193	0.0194	0.0193	0.0194	0.0212	0.0212	0.0194	0.0212	
rho_eff	0.0464	0.0777	0.0771	0.0777	0.0847	0.0847	0.0777	0.0847	
G _f	0.1458	0.1499	0.1418	0.1468	0.1478	0.1479	0.1478	0.1480	N/mm
s _{rm}	179.90	179.90	179.90	179.90	179.90	179.90	179.90	179.90	mm
n	1.292	1.275	1.308	1.275	0.897	0.897	1.275	0.897	
f _{ct}	4.82	5.28	4.42	4.93	5.03	5.04	5.04	5.05	MPa
E _s	28990	28640	28640	28640	28390	28390	28640	28390	MPa
E _o	37450	36510	37450	36510	25470	25470	36510	25470	MPa
V	473.60	507.45	448.35	475.95	471.30	457.05	475.05	451.20	kN
M	369.41	395.81	349.71	371.24	367.61	356.50	371.01	351.94	kN-m
z	203.31	203.16	203.44	203.16	198.38	198.38	203.16	198.38	mm
I _{total}	2.49E+09	2.48E+09	2.51E+09	2.48E+09	2.16E+09	2.16E+09	2.48E+09	2.16E+09	mm ⁴
d(b,crit)	19.383	16.662	22.584	18.729	19.504	19.435	18.026	19.394	1 mm
x'	14.547	15.032	14.206	14.955	16.166	16.705	15.302	16.943	2 mm
eps _s	0.00174	0.00186	0.00165	0.00174	0.00162	0.00157	0.00174	0.00155	3 -

Figure B.14: Shear stress calculation along the cross-section of coupled members after crack-1 (using Tung ang Tue's theory)

Coupled Members									
		Slab no. 8	Slab no. 7	Slab no. 6	Slab no. 5	Slab no. 4	Slab no. 3	Slab no. 2	Slab no. 1
d		257	257	257	257	257	257	257	257
a		780	780	780	780	780	780	780	780
d/b.critl	$0.5 \cdot (100 \cdot \rho) \cdot \sqrt{0.9 / f_c}$	19.383	16.662	22.584	18.729	19.504	19.435	18.026	19.394
x'	$(\text{eps_ct} / \text{eps_s}) \cdot (d - x)$	14.547	15.032	14.206	14.955	16.166	16.705	15.302	16.943
eps_s	$(1 / E_s \cdot \rho \cdot b \cdot d^2) \cdot (M / z + V \cdot l / 2)$	0.00174	0.00186	0.00165	0.00174	0.00162	0.00157	0.00174	0.00155
x	$(\text{SQRT}((\rho \cdot \eta)^2 + 2 \cdot \rho \cdot \eta) - \rho \cdot \eta) \cdot d$	104.725	105.345	105.064	105.345	109.105	109.105	105.345	109.105
x''	$(G / f) \cdot (f_{ct} \cdot w_k) \cdot (d - x \cdot x')$	10.120	9.122	10.200	9.509	9.001	8.953	9.361	8.930
w_k	$s_{rm} / E_s \cdot (\text{Sigma}_s - 0.5 \cdot (f_{ct} / \rho \cdot \eta \cdot \text{eff}) \cdot (1 + \eta \cdot \rho \cdot \eta \cdot \text{eff}))$	0.412	0.425	0.433	0.429	0.430	0.430	0.428	0.430
sigma_xm	$f_{ct} \cdot (1 - 0.5 \cdot (d_{b.critl} / x + x''))$	2.926	3.458	2.378	3.040	3.083	3.134	3.196	3.157
	$f_{ct} \cdot (0.5 \cdot (d_{b.critl} / x + x''))$								
tau_u	$\text{sqrt}(f_{ct} \cdot (f_{ct} - \text{sigma}_x m))$	3.021	3.100	3.010	3.047	3.133	3.104	3.044	3.092
tau_max	$\text{tau}_u / (1 - (x' / x) \cdot \eta^2)$	3.081	3.164	3.066	3.110	3.203	3.178	3.110	3.168
tau_rc	$(2/3 \cdot \text{tau}_u \cdot \text{max}(x + 1/2 \cdot (\text{tau}_u \cdot \text{max} + \text{tau}_u) \cdot x + \text{tau}_u \cdot u \cdot (d - x \cdot x')) / d)$	2.629	2.696	2.616	2.650	2.712	2.688	2.648	2.678
V_rc	$\text{tau}_u \cdot \text{rc} \cdot b \cdot d$	675.579	692.799	672.374	680.997	696.948	690.873	680.630	688.313
x_0	$M_{cr} / P + s_{cr} m(1.3 - M_{max} / M_y)$	304.72	306.87	301.45	306.22	296.04	299.91	309.15	301.62
x' + x''		24.667	24.154	24.407	24.464	25.167	25.658	24.663	25.873
		42.65%	36.53%	49.97%	43.08%	47.88%	51.16%	43.09%	52.55%
M_cr		59.11504	64.43094	54.49901	60.12312	54.73739	54.85179	61.47734	54.9194

Figure B.15: Shear stress calculation along the cross-section of coupled members after crack-2 (using Tung and Tue's theory)

	Slab no. 8	Slab no. 7	Slab no. 6	Slab no. 5	Slab no. 4	Slab no. 3	Slab no. 2	Slab no. 1
	300	300	300	300	300	300	300	300
	280	280	280	280	280	280	280	280
	260	260	260	260	260	260	260	260
Interface	240							
x	220	220	220	220	220	220	220	220
x+x'	195.2751	194.6554	194.9357	194.6554	190.8952	190.8952	194.6554	190.8952
x+x'+x''	180.7283	179.6234	180.7293	179.7001	174.7287	174.1898	179.3536	173.9523
d	170.6085	170.5016	170.5291	170.1913	165.7278	165.2369	169.9927	165.0222
	0	0	0	0	0	0	0	0
d_b_crit	19.38306	16.66161	22.58365	18.7289	19.50386	19.43461	18.02581	19.39392
x'+x''	24.66662	24.15377	24.40661	24.46412	25.1674	25.6583	24.66267	25.87297
(x'+x''-d_b_crit)/2	2.64178	3.74608	0.91148	2.86761	2.831769	3.11844	3.318431	3.239527
	173.2502	174.2477	171.4406	173.0589	168.5595	168.3487	173.3112	168.2617
0	0	0	0	0	0	0	0	0
	1.064	1.087	1.056	1.069	1.067	1.058	1.069	1.055
	1.904	1.947	1.890	1.913	1.918	1.903	1.913	1.897
Interface	2.519	2.578	2.502	2.534	2.555	2.535	2.534	2.526
	2.909	2.981	2.891	2.930	2.975	2.952	2.930	2.943

Figure B.16: Shear stress along the cross-section of coupled members after crack after some interpolation-1

Bibliography

- [1] A. Muttoni and M. F. Ruiz, *Shear strength of members without transverse reinforcement as function of critical shear crack width*, ACI Structural Journal **105**, 163 (2008).
- [2] Y. Yang, J. Walraven, and J. d. Uijl, *Shear behavior of reinforced concrete beams without transverse reinforcement based on critical shear displacement*, Journal of Structural Engineering **143**, 04016146 (2016).
- [3] Y. Yang, *Shear behaviour of reinforced concrete members without shear reinforcement: A new look at an old problem*, (2014).
- [4] J. Kepler, *1. Ziele und Ergebnisse* $\frac{3}{4}$, , 1 (2015).
- [5] N. D. Tung and N. V. Tue, *A new approach to shear design of slender reinforced concrete members without transverse reinforcement*, Engineering structures **107**, 180 (2016).
- [6] Z. P. Bažant and A. B. Wahab, *Stability of parallel cracks in solids reinforced by bars*, International Journal of Solids and Structures **16**, 97 (1980).
- [7] J. C. Walraven, *Fundamental analysis of aggregate interlock*, Journal of the Structural Division **107**, 2245 (1981).
- [8] E. Mörsch and E. P. Goodrich, *Concrete-steel Construction:(Der Eisenbetonbau)* (Engineering News Publishing Company, 1910).
- [9] T. Baumann and H. Rüschi, *Versuche zum studien der verdübelungswirkung der biegezugbewehrung eines stahlbetonbalkens* (Ernst, 1970).
- [10] A. Mphonde, *Aggregate interlock in high strength reinforced concrete beams*, in *Proceedings of the Institution of Civil Engineers*, Vol. 85 (1988).
- [11] B. Belletti, C. Damoni, M. Hendriks, and J. Den Uijl, *Nonlinear finite element analysis of reinforced concrete slabs: Comparison of safety formats*, in *FraMCoS-8: Proceedings of the 8th International Conference on Fracture Mechanics of Concrete and Concrete Structures, Toledo, Spain, 10-14 March 2013* (International Center for Numerical Methods in Engineering, 2013).